J. Fluid Mech. (2010), *vol.* 653, *pp.* 391–429.
doi:10.1017/S0022112010000364

Asymptotic theory of the elastohydrodynamic adhesion and gliding motion of a solid particle over soft and sticky substrates at low Reynolds numbers

JAVIER URZAY†

Department of Mechanical and Aerospace Engineering, University of California San Diego, La Jolla, CA 92093-0411, USA

(Received 23 June 2009; revised 15 January 2010; accepted 15 January 2010; first published online 5 May 2010)

This analysis makes use of asymptotic analyses and numerical methods to address, in the limit of small Reynolds and ionic Péclet numbers and small clearances, the canonical problem of the forces exerted on a small solid spherical particle undergoing slow translation and rotation in an incompressible fluid moving parallel to an elastic substrate, subject to electric double-layer and van der Waals intermolecular forces, as a representative example of particle gliding and the idealized swimming dynamics of more complex bodies near soft and sticky surfaces in a physiological solvent. The competition of the hydrodynamic, intermolecular and surface-deformation effects induces a lift force, and drag-force and drift-force perturbations, which do not scale linearly with the velocities, and produce a non-additivity of the intermolecular effects by reducing the intensity of the repulsive forces and by increasing the intensity of the attractive forces. The lift force enhances a reversible elastohydrodynamic adhesion regime in both ionized and deionized solvents, in which lateral motion and lift-off from the substrate can occur. An irreversible elastohydrodynamic adhesion regime, produced by elastic instabilities in the form of surface bifurcations in the substrate, is found to exist for both positive and negative lift forces and is enhanced by small gliding velocities and large substrate compliances, for which critical thresholds are calculated for both ionized and deionized solvents. Elastohydrodynamic corrections are derived for the critical coagulation concentration of electrolyte predicted by the Derjaguin–Landau–Verwey–Overbeek (DLVO) standard theory of colloid stabilization. The corrected DLVO critical concentration is unable to describe the adhesion process when the substrate is sufficiently compliant or when the solvent is deionized. These effects may have consequences on the lateral motility and adhesion of small particles and swimming micro-organisms to soft and sticky substrates, in which the reversible or irreversible character of the adhesion process may be influenced not only by the solvent ionic strength, as described by the DLVO theory, but also by the motion kinematics and the substrate mechanical properties.

1. Introduction

Soft materials can be deformed by the action of external forces (Landau & Lifshitz 1959; Johnson 1985). Nearby substrate deformations produced by hydrodynamic and intermolecular forces induce nonlinearities on the otherwise linear equations of

† Email address for correspondence: jurzay@ucsd.edu

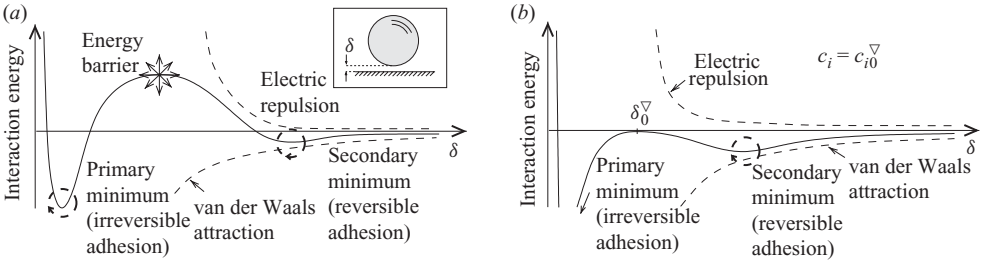

FIGURE 1. Sketch of typical particle–surface interaction energy curves in the DLVO theory, adapted from Israelachvili (1985), for (*a*) low and (*b*) high (critical coagulation) concentration of electrolyte in the solvent.

viscous fluid motion at low Reynolds numbers and produce forces on submerged moving particles and swimmers that may serve as representative sources of lateral motility at small scales and may also suppress adhesion. However, such deformations may as well enhance adhesion if the internal restoring force of the substrate is not sufficiently large to outweigh the resulting hydrodynamic and intermolecular traction stresses on its surface.

The study of the intermolecular and viscous hydrodynamic interactions between solids and soft substrates may be of some interest from a biology perspective. Motivated by the practical importance of the control and suppression of biofilm growth on surfaces, adhesion of motile bacteria to rigid substrates has been previously analysed by accounting for electric and van der Waals forces (Vigeant, Ford & Wagner 2005). The study of the distinguished balance between these two interactions is the subject of the celebrated Derjaguin–Landau–Verwey–Overbeek (DLVO) theory (Derjaguin & Landau 1941; Verwey & Overbeek 1948), which is regarded as the fundamental theory of the stabilization and adhesion of lyophobic particles, although this theory may need to be modified to account for hydrodynamic effects and to accurately describe the phenomena of bacterial adhesion (Vigeant *et al.* 2005; Berke *et al.* 2008). Earlier work (Vigeant *et al.* 2005) identified reversible (short residence times and lateral motility) and irreversible (long residence times and sessility) adhesion modes, which depended on the ionic strength in the solvent. The reversible adhesion mode exemplifies a gliding motion along the surface in which the bacteria are momentarily entrapped in an accessible potential minimum, whereas the irreversible mode is experimentally observed as a 'sudden death' of the bacteria when they fall into the primary minimum, a region dominated by Born repulsion and steric forces, once the energy barrier becomes small at sufficiently large electrolyte concentrations, as shown in figure 1. Effects of surface chemical heterogeneities have been previously proposed as precursors of lateral immobilization and irreversible adhesion (Busscher, Poortinga & Bos 1998). In a more general situation, the presence of a nearby soft interface has been proved to produce kinematically irreversible forces on swimming bodies and moving particles at low Reynolds numbers (Berdan & Leal 1981; Skotheim & Mahadevan 2005; Weekley, Waters & Jensen 2006; Urzay, Llewellyn-Smith & Glover 2007; Trouilloud *et al.* 2008), which may modify their adhesion behaviour; the velocity scaling of these forces departs from the linear, kinematically reversible Stokesian velocity scaling of the hydrodynamic forces in viscous flows bounded by rigid surfaces, in which it produces direction-invariant forces under velocity-direction reversals. The near-contact motion of micro-organisms close to soft living tissues may be inevitably influenced by a number of complexities involving biochemical, intermolecular and hydrodynamic interactions and surface deformations

upon adhesion, but the study of simplified analytical models may still be warranted for shedding some modest amount of light into these intricacies.

From a general engineering standpoint, electric and van der Waals intermolecular forces are inherently present in the near-contact dynamics of liquid and solid interfaces, and are perhaps the most important contribution to the forces involved in the coagulation of colloids, bubble and droplet coalescence, physical adsorption and adhesion of particles to substrates (Israelachvili 1985; Lyklema 2005). Although the van der Waals forces between two atoms or molecules decrease with the seventh power of the separation distance, the forces between large molecular assemblies, such as spheres or plates, decrease with the second or third power of the separation distance, so that the effects of these interactions between macroscopic bodies prove to be still appreciable at a moderately long range (0.1 μm or more) (Israelachvili 1985; Lyklema 2005). Dispersion and coagulation of a suspension of particles may occur depending on the relative intensity of the electric double-layer and van der Waals forces, the balance of which is mainly modulated by the ionic strength in the solvent (Derjaguin & Landau 1941; Verwey & Overbeek 1948). Similarly, sheared concentrated suspensions of dense polymer microgel pastes display a slip behaviour beyond a critical sliding stress that is thought of being produced by a combination of elastohydrodynamic and intermolecular effects (Meeker, Bonnecaze & Cloitre 2004; Seth, Cloitre & Bonnecaze 2008).

Earlier pioneering works on the viscous motion of a cylinder near soft and non-sticky surfaces by Skotheim & Mahadevan (2005), and the near-contact dynamics of a sphere near a rigid wall by Goldman, Cox & Brenner (1967*b*), O'Neill & Stewartson (1967) and Cooley & O'Neill (1968), are generalized in this investigation by addressing the canonical problem of the forces exerted on a small spherical particle undergoing slow translation and rotation in a perfect liquid near a soft substrate, subject to electric and van der Waals intermolecular forces. Forces produced by the triple interaction of hydrodynamic, intermolecular and substrate-deformation effects are derived, and novel limiting conditions for adhesion, based on critical substrate-mechanical properties, gliding velocities and electrolyte concentrations, are obtained in this analysis by making use of asymptotic analyses and numerical methods.

The paper is organized into seven additional sections and two appendices. Section 2 is dedicated to a general formulation of the problem, within the framework of a hydrodynamic lubrication model. Then, in the limit of nearly rigid substrates, an asymptotic scheme of the problem is proposed in § 3. Section 4 summarizes the main characteristics of the leading-order solution for rigid substrates. The second-order problem, which corresponds to the first perturbation of the wall deformation, is solved in § 5, analytical formulas for the elastohydromolecular forces are derived in the nearly rigid wall asymptotic limit and they are compared to numerical simulations, which are further extended to order-unity dimensionless substrate compliances. Elastohydrodynamic adhesion regimes and the lift-off process from the substrate are addressed in § 6. Section 7 is dedicated to the influences of the substrate mechanical properties. Finally, conclusions are drawn in § 8. Appendix A provides a mathematical description of the substrate mechanics, and Appendix B analyzes the simpler problem of the elastostatic adhesion mechanism of a stationary sphere produced by surface bifurcations on the soft substrate.

2. Formulation

A rigid spherical particle of radius a and dielectric constant ε_s translates at constant velocity U along the x axis, and rotates at constant angular velocity Ω about an axis

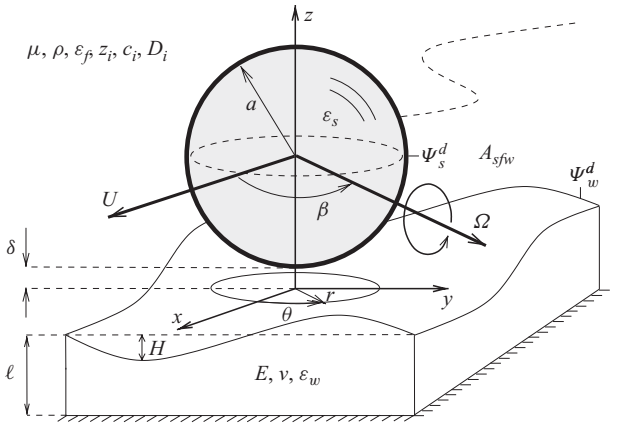

FIGURE 2. The model problem. The soft substrate is deformed by the hydrodynamic, electric and van der Waals intermolecular forces between the sphere and wall surfaces. Cases $\beta = 0$ and $\beta = \pi/2$ represent corkscrew and purely rolling motions, respectively.

orientated at an arbitrary azimuth angle β with respect to the translation axis, with both axes parallel to the unperturbed wall surface as depicted in figure 2, in this way representing a general drift motion on the horizontal plane. The sphere is immersed in a Newtonian incompressible fluid, which corresponds to an aqueous symmetric electrolyte of density ρ, equal to that of the sphere, viscosity μ, ionic valency z_i, ionic diffusion coefficient D_i and dielectric constant ε_f. The clearance or minimum gap distance between the sphere and the unperturbed wall surface is $\delta = \epsilon a$, with $\epsilon \ll 1$ a small parameter. The ionic concentration in the bulk electrolyte far from the sphere is denoted by c_i. The soft substrate comprises an elastic layer of thickness ℓ, dielectric constant ε_w, Young modulus E and Poisson coefficient ν, and is bonded to a rigid motionless substrate. The ratio of the characteristic surface deflection H_c, produced by the hydrodynamic stress, to the minimum clearance δ is defined as the softness parameter, elastoviscous number or hydrodynamic compliance $\eta = H_c/\delta$. The motion can be considered steady in the reference frame shown in figure 2 as long as the time scale of the sphere motion, δ/U, is much longer than the viscous time scale, δ^2/ν, which is also much longer than the substrate response time scale, δ/c, where c is the speed of sound in the substrate. Then, the Reynolds numbers of translation and rotation are small, $Re_U = \rho U a/\mu \ll 1$ and $Re_\Omega = \omega Re_U \ll 1$, so that the flow can be described by the Stokes equations to leading order. In this formulation, $\omega = \Omega a/U$ is a kinematic parameter that measures the ratio of the rotational to the translational peripheral velocities.

The conservation equations are non-dimensionalized with a as the unit of length, H_c as the unit of surface deflection, $U\mathscr{V}(\omega, \beta)$ as the unit of velocity and $\mu U\mathscr{V}(\omega, \beta)/a$ as the unit of pressure, where

$$\mathscr{V}(\omega, \beta) = |\boldsymbol{e_x} - \boldsymbol{\omega} \times \boldsymbol{e_z}| = \sqrt{1 + \omega^2 + 2\omega \sin\beta} \tag{2.1}$$

is a characteristic non-dimensional velocity in the clearance, with $\boldsymbol{e_i}$ as unit vectors, and $\boldsymbol{\omega} = \boldsymbol{\Omega} a/U$. Thus, hereafter the velocity $U\mathscr{V}(\omega, \beta)$ is referred to as the 'gliding velocity'. In these variables, and in an inertial reference frame translating with the sphere, the mass and momentum conservation equations for the velocity $\boldsymbol{v}$ and

hydrodynamic pressure P become

$$\left.\begin{aligned}\nabla\cdot\boldsymbol{v}&=0,\\ -\nabla P+\nabla^2\boldsymbol{v}&=0,\end{aligned}\right\}\tag{2.2}$$

subject to non-slip boundary conditions on the sphere and substrate surfaces, where the velocity respectively is

$$\boldsymbol{v}=\frac{\omega(z-1-\epsilon)\sin\beta}{\mathscr{V}(\omega,\beta)}\boldsymbol{e_x}-\frac{\omega(z-1-\epsilon)\cos\beta}{\mathscr{V}(\omega,\beta)}\boldsymbol{e_y}+\frac{\omega(y\cos\beta-x\sin\beta)}{\mathscr{V}(\omega,\beta)}\boldsymbol{e_z},\tag{2.3}$$

and

$$\boldsymbol{v}=-\frac{\boldsymbol{e_x}}{\mathscr{V}(\omega,\beta)}+\frac{\eta\epsilon(\nabla_\perp H\cdot\boldsymbol{e_x})}{\mathscr{V}(\omega,\beta)}\boldsymbol{e_z}.\tag{2.4}$$

In this formulation, $\nabla_\perp$ is the two-dimensional gradient operator in x and y. The second term on the right-hand side of (2.4) represents the vertical fluid entrainment induced by the surface-deformation field, which remains stationary in this reference frame.

A lubrication approximation can be obtained for $\epsilon\ll1$ by defining the inner velocities $v_r'=v_r$, $v_\varphi'=v_\varphi$ and $v_z'=v_z\epsilon^{-1/2}$, the inner hydrodynamic pressure $P'=P\epsilon^{3/2}$ and the inner coordinates $z'=z/\epsilon$ and $r'=r/\epsilon^{1/2}$. The surface of the sphere in the gap region is given by (dropping primes)

$$h_0(r)=1+r^2/2+O(\epsilon).\tag{2.5}$$

In these variables, a regular expansion in powers of ϵ yields, to leading order, the conservation equations

$$\left.\begin{aligned}&\frac{1}{r}\frac{\partial}{\partial r}(rv_r)+\frac{1}{r}\frac{\partial v_\varphi}{\partial\varphi}+\frac{\partial v_z}{\partial z}=0,\\ &\frac{\partial P}{\partial r}=\frac{\partial^2 v_r}{\partial z^2},\quad \frac{1}{r}\frac{\partial P}{\partial\varphi}=\frac{\partial^2 v_\varphi}{\partial z^2},\quad \frac{\partial P}{\partial z}=0,\end{aligned}\right\}\tag{2.6}$$

subject to

$$v_r=-\cos\varphi+\frac{\cos(\varphi-\gamma)}{\mathscr{V}(\omega,\beta)},\quad v_\varphi=\sin\varphi-\frac{\sin(\varphi-\gamma)}{\mathscr{V}(\omega,\beta)},\quad v_z=-r\cos\varphi+\frac{r\cos(\varphi-\gamma)}{\mathscr{V}(\omega,\beta)},\tag{2.7}$$

on the sphere surface $z=h_0(r)$, and

$$v_r=-\frac{\cos(\varphi-\gamma)}{\mathscr{V}(\omega,\beta)},\quad v_\varphi=\frac{\sin(\varphi-\gamma)}{\mathscr{V}(\omega,\beta)},\quad v_z=\frac{\eta\nabla_\perp H\cdot\boldsymbol{e_x}}{\mathscr{V}(\omega,\beta)},\tag{2.8}$$

on the wall surface $z=-\eta H$. In this formulation, θ is the physical azimuth angle (measured from the x axis as shown in figure 2), and

$$\varphi=\theta+\gamma\tag{2.9}$$

is a reduced angle, with $\gamma(\omega,\beta)$ as a phase angle of the gap pressure distribution given by

$$\gamma(\omega,\beta)=\arctan\left(\frac{\omega\cos\beta}{1+\omega\sin\beta}\right),\tag{2.10}$$

with $-\pi/2\leqslant\gamma\leqslant\pi/2$. For a purely rolling motion, $\beta=\pi/2$ and $\gamma=0$, so that $\varphi=\theta$ and the pressure distribution is dominated by the entrainment of fluid taking place along the $\theta=0$ axis. For corkscrew motion, $\beta\to0$ and $\gamma\sim\arctan\omega$, so that as ω increases the peak pressures are expected to be increasingly dominated by the

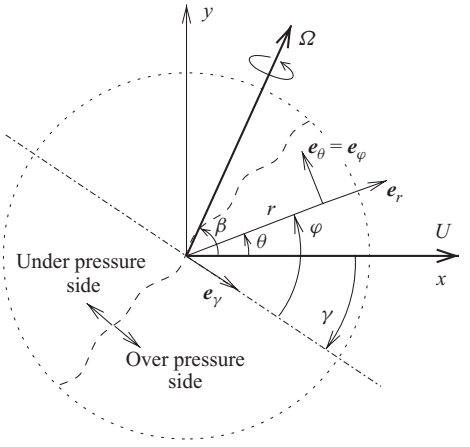

FIGURE 3. Top view of the gap region showing the spatial orientation of the polar azimuth angle θ, phase angle γ and reduced angle φ.

lateral fluid entrainment enhanced by the rotational motion, shifting the pressure peaks towards the line $\theta = -\gamma$. The rotated system of coordinates (r, φ, z) is shown in figure 3 and constitutes a valuable asset for the simplification of the analytical and numerical integration of the problem as further detailed below.

The surface location and the vertical velocity there render the problem (2.6)–(2.8) nonlinear. Continuity equation may still be used to eliminate the velocities after integrating the momentum equations, which yields the Reynolds equation

$$\frac{\partial}{\partial r}\left(r\frac{\partial P}{\partial r}h^3 + 6rh\cos\varphi\right) + \frac{1}{r}\frac{\partial}{\partial \varphi}\left(\frac{\partial P}{\partial \varphi}h^3 - 6rh\sin\varphi\right) = 0, \tag{2.11}$$

with $h = h_0(r) + \eta H$ the gap profile. Equation (2.11) is subject to the boundedness and periodicity conditions

$$|P| < \infty \quad \text{at} \quad r = 0, \quad P \to 0 \quad \text{at} \quad r \to \infty, \quad P|_{\varphi=0} = P|_{\varphi=2\pi}, \quad \left.\frac{\partial P}{\partial \varphi}\right|_{\varphi=0} = \left.\frac{\partial P}{\partial \varphi}\right|_{\varphi=2\pi}. \tag{2.12}$$

Note that the velocity scaling and azimuth angle redefinition given by (2.1) and (2.9) renders the nonlinear partial differential problem (2.11) and (2.12) independent of ω and β, so that pressure solutions $P(r, \varphi)$ obtained by integration of (2.11) and (2.12) are valid for any rotation rate ω and rotation azimuthal orientation β, thus reducing the space of solutions by two dimensions.

The radial and azimuth velocity fields in the gap correspond to a combination of Couette and Poiseuille flows:

$$\left.\begin{aligned} v_r &= \frac{1}{2}\frac{\partial P}{\partial r}\left\{z^2 - z\left[h_0(r) - \eta H\right] - \eta H h_0(r)\right\} \\ &\quad - \left[\cos\varphi - \frac{2\cos(\varphi-\gamma)}{\mathscr{V}(\omega,\beta)}\right]\left[\frac{z+\eta H}{h_0(r)+\eta H}\right] - \frac{\cos(\varphi-\gamma)}{\mathscr{V}(\omega,\beta)}, \\ v_\varphi &= \frac{1}{2r}\frac{\partial P}{\partial \varphi}\left\{z^2 - z\left[h_0(r) - \eta H\right] - \eta H h_0(r)\right\} \\ &\quad + \left[\sin\varphi - \frac{2\sin(\varphi-\gamma)}{\mathscr{V}(\omega,\beta)}\right]\left[\frac{z+\eta H}{h_0(r)+\eta H}\right] + \frac{\sin(\varphi-\gamma)}{\mathscr{V}(\omega,\beta)}, \end{aligned}\right\} \tag{2.13}$$

and the vertical velocity is obtained by integrating the mass conservation equation

$$v_z = \int_z^{h_0(r)} \left[\frac{1}{r} \frac{\partial}{\partial r}(r v_r) + \frac{1}{r} \frac{\partial v_\varphi}{\partial \varphi} \right] \mathrm{d}z + v_z \Big|_{z=h_0(r)}, \tag{2.14}$$

with the three velocity components expressed in the (r, φ, z) system of coordinates.

2.1. *The electric double-layer and van der Waals pressures*

The van der Waals forces arise from the interaction between permanent polar molecules (Keesom orientation force), permanent polar and polarizable molecules (Debye induction force) and non-polar but polarizable molecules (London dispersion force). In contrast to other type of forces that may be present depending on the particular properties of the molecules, the London dispersion interactions are always present because of quantum-mechanical effects between fluctuating electron clouds, and they are not easily screened by polar solvents. Using the Derjaguin approximation (Derjaguin 1934), the effect of this interaction is assumed to result in a non-retarded disjoining pressure or intermolecular compression stress Π^{vdW} that represents the excess pressure in the gap compared to that of the bulk flow P. The disjoining pressure acts as an additional compression stress on both the sphere and wall surfaces, and its non-dimensional magnitude is

$$\Pi^{vdW} = -\frac{\Upsilon}{h^3}, \tag{2.15}$$

with

$$\Upsilon = \frac{A_{sfw}}{6\pi\mu U \mathscr{V}(\omega, \beta) a^{1/2} \delta^{3/2}} \tag{2.16}$$

as the ratio of the van der Waals to hydrodynamic characteristic stresses. In this formulation, A_{sfw} is the Hamaker coefficient, which depends on the particle, fluid and wall dielectric constants and absorption spectra, and typically ranges from 1 to 100 times the thermal energy kT, with k as the Boltzmann constant and T as the temperature (Israelachvili 1985; Lyklema 2005). The sign of the Hamaker coefficient is the same as the sign of the product of the excess polarizabilities $\varepsilon_s - \varepsilon_f$ and $\varepsilon_w - \varepsilon_f$ (Lifshitz 1956). If the dielectric constant of the liquid ϵ_f is intermediate between ϵ_w and ϵ_s, the van der Waals force is repulsive, and attractive otherwise. The van der Waals interactions are commonly attractive due to the high dielectric constant of usual solvents.

The van der Waals forces alone do not usually determine the total intermolecular interaction, except in vacuum or deionized solvents. In aqueous electrolyte solutions, electroneutral solid surfaces may become spontaneously charged even under no externally applied electric field. Specific ions are preferentially adsorpted by the surface because of non-electrical affinity interactions with its molecules, while others form an atmosphere of ions in rapid thermal motion in a thin cloud of thickness of $O(\ell_D)$ close to the surface, where ℓ_D is the Debye length, in such a way that the charged cloud and surface charge form an electroneutral system. Associated with this spontaneous formation of the double layer is a decrease of the Gibbs free energy, which ultimately leads to a combination of an osmotic overpressure and Maxwell stresses in the gap, with their total contribution classically represented by a disjoining

pressure or electric compression stress Π^{el} given by (Derjaguin 1934)

$$\Pi^{el} = \Xi \mathrm{e}^{-\kappa(h-1)}, \tag{2.17}$$

with

$$\Xi = \frac{64\delta^{3/2} c_i N_A kT}{\mu U \mathscr{V}(\omega, \beta) a^{1/2}} \lambda\left(\Psi_w^d, \Psi_s^d\right) \mathrm{e}^{-\kappa} \tag{2.18}$$

as the ratio of the electric to hydrodynamic characteristic stresses, and

$$\kappa = \frac{\delta}{\ell_D} = \sqrt{\frac{2(z_i \mathrm{e}\delta)^2 c_i N_A}{\varepsilon_0 \varepsilon_f kT}} \tag{2.19}$$

is the Debye–Hückel parameter. The function $\lambda(\Psi_w^d, \Psi_s^d)$ is given by (Lyklema 2005)

$$\lambda\left(\Psi_w^d, \Psi_s^d\right) = \tanh\left(z_i \Psi_w^d/4\right) \tanh\left(z_i \Psi_s^d/4\right). \tag{2.20}$$

Equation (2.17) represents the non-dimensional electric pressure for the interaction of two double layers of a symmetric electrolyte solution of concentration c_i. In this model, Ψ_s^d and Ψ_w^d are the non-dimensional Stern potentials (which are approximately similar to the zeta potentials) of the sphere and substrate surfaces respectively, which are assumed to be constant and are non-dimensionalized with the thermal voltage $kT/e \sim 25\,\mathrm{mV}$. Additionally, in this formulation e is the protonic charge, ε_0 is the permittivity of vacuum and N_A is the Avogadro's number. At constant and symmetric zeta potentials, the double-layer interaction results in a repulsive force, because, as the particle approaches the wall, ions must be driven off the substrate to decrease the surface charge, which in turn is proportional to the gradient of the electric potential on the surface; this forced discharge results in an increase of Gibbs free energy. More involved models of electric double-layer pressures could be used here, which may include important effects such as charge regulation due to surface chemical equilibrium constraints (Israelachvili 1985; Lyklema 2005), or surface permeability to ionic fluxes, which is believed to influence bacterial adhesion by ion-channelling effects in bacterial walls (Poortinga *et al.* 2002). Nonetheless, (2.17) represents a good and logical starting point for the present investigation.

Earlier work by Bike & Prieve (1995) found that the pressure gradient in the gap between a sliding sphere and a planar wall may distort the electric double-layer equilibrium configuration described above, producing an electro-osmotic flow of ions near both surfaces and a streaming potential in the gap, which in turn generate an electrokinetic lift on the particle. Electrokinetic interactions are found to be comparable to intermolecular forces only for highly viscous, low-conductivity solutions such as 95 % glycerol–water mixtures (Wu, Warszynksi & van de Ven 1995), for which the ionic Péclet number $Pe_i = U\mathscr{V}\delta/D_i$ is of order unity or larger, with D_i as the ionic diffusion coefficient. In this investigation, electrokinetic forces produced by pressure gradients are neglected since the characteristic diffusion time of the ions in the gap, δ^2/D_i, is assumed to be much smaller than the characteristic time of translational or rotational motion, $\delta/U\mathscr{V}$, so that $Pe_i \ll 1$ and the perturbation of the equilibrium electric double-layer produced by the convective transport of ions can be neglected in the first approximation. This simplification leads to a Boltzmann distribution of ionic concentration in the gap, from which the electric pressure (2.17) is derived by solving the corresponding Poisson–Boltzmann equation (Lyklema 2005). The condition $Pe_i \ll 1$ is easily satisfied by typical highly conductive physiological solutions (mostly containing Na^+, K^+, Cl^-, Ca^{2+} and Mg^{2+}), for which the ionic

diffusion dominates and the electrokinetic lift on the sphere is at least three to four orders of magnitude smaller than the elastohydromolecular forces resulting from the present analysis.

For convenience, the hydromolecular pressure $P^\star$ is defined as

$$P^\star = P + \Pi^{vdW} + \Pi^{el}, \tag{2.21}$$

which represents the net compression normal stress (hydrodynamic and intermolecular) acting on the sphere and substrate surfaces. The hydromolecular pressure $P^\star$ is, in general, a function of the intermolecular and kinematic parameters, the fluid and wall mechanical properties and the spatial coordinates.

Equations (2.11), (2.12), (2.15) and (2.17) need to be supplied with an appropriate substrate mechanical model. The substrate mechanics is analysed in Appendix A.

2.2. *Effects of ionic strength: the critical coagulation concentration*

In the framework of the classic DLVO theory, sufficiently large electrolyte concentrations c_i may lead to a double-layer compression effect, by which the Debye thickness ℓ_D decreases with increasing c_i and the particle can approach a shorter distance before any repulsion is felt. Further approach produces a large attracting van der Waals force on the particle able to outweigh any repulsion. This leads to rapid coagulation if the energy barrier to the irreversible adhesion minimum becomes smaller than the energy associated with Brownian perturbations of the gap distance. The critical concentration for the rapid coagulation of a sphere on a flat rigid substrate is given by the system of equations

$$F_z(\delta^\triangledown) = 0 \quad \text{and} \quad \int_{\delta^\triangledown}^{\infty} F_z(\delta)\,\mathrm{d}\delta \approx bkT, \tag{2.22}$$

where F_z is the net intermolecular force on the sphere and b is a constant, which is conventionally set to $b = 0$ for a small energy barrier (Verwey & Overbeek 1948). Equation (2.22) represents the coagulation event or irreversible adhesion in the primary minimum as sketched in figure 1, and they give the critical conditions for which the force on the particle is zero while the work produced by a random perturbation of the gap distance against the normal force is roughly a multiple of the thermal energy of the surrounding molecules. When F_z is obtained by the classic DLVO theory, these expressions yield the critical coagulation concentration

$$c_{i0}^\triangledown = 73728\pi^2 \mathrm{e}^{-2} \frac{(\varepsilon_0\varepsilon_f)^3(kT)^5\lambda^2(\Psi_w^d, \Psi_s^d)}{(z_i e)^6 A_{sfw}^2 N_A} \tag{2.23}$$

(Lyklema 2005). The minimum clearance for coagulation, $\delta_0^\triangledown$, measured with respect to the Debye layer thickness based on c_{i0}, is given by $\kappa_0^\triangledown = \delta_0^\triangledown/\ell_{D0}^\triangledown = 1$.

As shown below, F_z is also influenced by hydrodynamic and substrate compliance effects, so that (2.23) needs to be correspondingly modified. Additionally, local substrate deformations produced by elastic instabilities of hydromolecular origin are found in this analysis to induce irreversible adhesion, an effect that is obliterated by simply using the criterion (2.22) and (2.23).

3. Nearly rigid-wall asymptotics and summary of main non-dimensional parameters

In this model, the characteristic area of the lubrication region is δ^2/ϵ, which, by the chordal theorem, is also roughly the area of the circular zone centred at

a distance $-\delta$ inside the sphere. This area is of the same order of magnitude as the effective interaction area of the van der Waals forces, and it is larger than the typical interaction area $\delta^2/\epsilon\kappa$ of the electric double-layer forces (Israelachvili 1985), since these decay exponentially in the radial direction with a slope proportional to κ, with $\kappa \geqslant O(1)$. It must be emphasized that, in this analysis, surface deformations are restrained to occur in the lubrication region. This assumption proves to be accurate if the characteristic deformation H_c is much smaller than the lubrication region size $\delta/\epsilon^{1/2}$, or equivalently, if the hydrodynamic compliance satisfies $\eta \ll 1/\epsilon^{1/2}$. Analyses for larger values of η may produce appreciable surface deformations outside the inner lubrication region, so that η may have to be incorporated in the inner scaling of the lubrication zone and an asymptotic matching may have to be performed with the outer viscous region as similarly performed in earlier works (O'Neill & Stewartson 1967; Cooley & O'Neill 1968) for the rigid-wall case.

The regular asymptotic expansions

$$\left.\begin{aligned} P^{\bigstar} &= P_0^{\bigstar} + \eta P_1^{\bigstar} + O(\eta^2), \\ h &= h_0(r) + \eta[H_0 + \eta H_1 + O(\eta^2)], \\ \boldsymbol{v} &= \boldsymbol{v_0} + \eta \boldsymbol{v_1} + O(\eta^2), \end{aligned}\right\} \tag{3.1}$$

are defined for slightly soft surfaces $\eta \ll 1$. The corresponding expansions of the van der Waals (2.15) and electric pressures (2.17) yield

$$\Pi^{vdW} = \Pi_0^{vdW} + \eta \Pi_1^{vdW} + O(\eta^2) = -\Upsilon/h_0^3(r) + 3\Upsilon H_0 \eta/h_0^4(r) + O(\eta^2) \tag{3.2}$$

and

$$\Pi^{el} = \Pi_0^{el} + \eta \Pi_1^{el} + O(\eta^2) = \Xi \mathrm{e}^{-\kappa[h_0(r)-1]} - \kappa \Xi \eta H_0 \mathrm{e}^{-\kappa[h_0(r)-1]} + O(\eta^2). \tag{3.3}$$

The van der Waals and electric compliances are defined as

$$\Delta^{vdW} = \eta\Upsilon, \qquad \text{and} \qquad \Delta^{el} = \eta\Xi, \tag{3.4}$$

and they represent the ratio of the intermolecular to the elastic characteristic stresses. The method for the calculation of Δ^{el}, Δ^{vdW} and η as a function of the dimensional parameters is detailed in Appendix A by the expressions (A 23)–(A 28).

In what follows, asymptotic solutions of (2.11)–(2.12) are sought in the nearly rigid-wall asymptotic (NRWA) limit: $\eta \ll 1$, $\Delta^{vdW} \ll 1$, $\Delta^{el} \ll 1$ and $\kappa \geqslant O(1)$. In this asymptotic limit, the elastic stress dominates over the intermolecular and hydrodynamic stresses on the substrate, which produce small surface deformations, with no clear limitation in the ratios of hydrodynamic to intermolecular stresses as long as they are sufficiently small such that the expansions (3.2) and (3.3) are asymptotic, $\Upsilon \ll 1/\eta$ and $\Xi \ll 1/\eta$.

Note that the NRWA limit may represent realistic physical conditions that may well be found in the hydrodynamics of small particles over soft materials. Table 1 summarizes the non-dimensional parameters introduced in the preceding sections and compares the asymptotic ordering required in the NRWA limit with typical values extracted from earlier studies in particle adhesion assuming a moderately soft material as a substrate. Nonetheless, the substrate compliances are highly nonlinear in the gap distance and inversely proportional to the substrate compliance, so that they are expected to rapidly attain $O(1)$ values upon adhesion and for softer materials.

Parameter	Substrate	Definition	Ordering	estimate
Hydrodynamic compliances				
η_0	Thin layer compressible	$\dfrac{\mu U \mathscr{V}(\omega,\beta)\ell a^{1/2}(1+\nu)(1-2\nu)}{E(1-\nu)\delta^{5/2}}$	$\ll 1$	0.05
η_2	Thin layer incompressible	$\dfrac{\mu U \mathscr{V}(\omega,\beta)\ell^3}{E a^{1/2}\delta^{7/2}}$	$\ll 1$	0.002
η_∞	Semi-infinite medium	$\dfrac{\mu U \mathscr{V}(\omega,\beta) a(1-\nu^2)}{\pi E\delta^2}$	$\ll 1$	0.08
van der Waals compliances				
Δ_0^{vdW}	Thin layer compressible	$\dfrac{A_{sfw}\ell(1+\nu)(1-2\nu)}{6\pi E(1-\nu)\delta^4}$	$\ll 1$	0.001
Δ_2^{vdW}	Thin layer incompressible	$\dfrac{A_{sfw}\ell^3}{6\pi a E\delta^5}$	$\ll 1$	0.00008
Δ_∞^{vdW}	Semi-infinite medium	$\dfrac{A_{sfw}a^{1/2}(1-\nu^2)}{6\pi^2 E\delta^{7/2}}$	$\ll 1$	0.002
Electric compliances				
Δ_0^{el}	Thin layer compressible	$\dfrac{64(1+\nu)(1-2\nu)\ell c_i N_A kT}{E(1-\nu)\delta}\lambda \mathrm{e}^{-\kappa}$	$\ll 1$	0.005
Δ_2^{el}	Thin layer incompressible	$\dfrac{64\ell^3 c_i N_A kT}{Ea\delta^2}\lambda \mathrm{e}^{-\kappa}$	$\ll 1$	0.0002
Δ_∞^{el}	Semi-infinite medium	$\dfrac{64a^{1/2}c_i N_A kT(1-\nu^2)}{\pi E\delta^{1/2}}\lambda \mathrm{e}^{-\kappa}$	$\ll 1$	0.008
Intermolecular–hydrodynamic stress ratios				
Υ	–	$\dfrac{A_{sfw}}{6\pi\mu U \mathscr{V}(\omega,\beta)a^{1/2}\delta^{3/2}}$	$\ll 1/\eta$	0.03
Ξ	–	$\dfrac{64\delta^{3/2}c_i N_A kT}{\mu U \mathscr{V}(\omega,\beta)a^{1/2}}\lambda \mathrm{e}^{-\kappa}$	$\ll 1/\eta$	0.1
Debye–Hückel parameter				
κ	–	$\sqrt{\dfrac{2(z_i e\delta)^2 c_i N_A}{\varepsilon_0\varepsilon_f kT}}$	$\geqslant O(1)$	10.3

TABLE 1. Fundamental non-dimensional parameters and their definition, their asymptotic ordering in the NRWA limit and numerical estimates, which are based on a particle of radius $a = 50\,\mu\mathrm{m}$ gliding at $U\mathscr{V} = 50\,\mu\mathrm{m\,s^{-1}}$. The parameters of the substrate are $E = 1\,\mathrm{kPa}$, $\ell = 0.5\,\mu\mathrm{m}$ (when finite), $\nu = 0$ (when compressible), $\nu = 0.5$ (when incompressible), $\delta = 0.1\,\mu\mathrm{m}$. The solvent is a symmetric monovalent aqueous electrolyte of $c_i = 1\,\mathrm{mM}$ NaCl, $z_i = 1$, $\rho = 1000\,\mathrm{kg\,m^{-3}}$, $\mu = 1$ mPa s, $\epsilon_f = 80$, $\Psi_s^d = \Psi_w^d = -2$ and $D_i = 10^{-9}$ $\mathrm{m^2\,s^{-1}}$. The Hamaker coefficient is $A_{sfw} = 1.5\,kT$, with $T = 300$ K. Typical values of the dimensional intermolecular parameters are obtained from Israelachvili (1985) and Lyklema (2005).

4. Hydrodynamic and intermolecular forces: the leading-order solution ($\eta = 0$)

To leading order in η, the intermolecular forces are decoupled from the hydrodynamic forces since there is no surface deformation. Integrating the electric and van der Waals pressures (2.15) and (2.17) over the vertical projection of the inner

element of the sphere surface $\mathrm{d}S_z = -a^2\epsilon r\mathrm{d}r\mathrm{d}\varphi\boldsymbol{e}_z$ yields

$$F_{z0}^{vdW} = -\frac{\mu U\mathscr{V}(\omega,\beta)a}{\epsilon^{1/2}}\int_0^{2\pi}\int_0^{\infty}\Pi_0^{vdW} r\,\mathrm{d}r\,\mathrm{d}\varphi = -\frac{\pi\mu U\mathscr{V}(\omega,\beta)a\Upsilon}{\epsilon^{1/2}} = -\frac{A_{sfw}a}{6\delta^2}, \quad (4.1)$$

and

$$\begin{aligned} F_{z0}^{el} &= \frac{\mu U\mathscr{V}(\omega,\beta)a}{\epsilon^{1/2}}\int_0^{2\pi}\int_0^{\infty}\Pi_0^{el} r\mathrm{d}\,r\mathrm{d}\varphi \\ &= \frac{2\pi\mu U\mathscr{V}(\omega,\beta)a\Xi}{\epsilon^{1/2}\kappa} = 128\pi a\ell_D c_i^{\infty}N_A kT\lambda(\Psi_w^d,\Psi_s^d)\mathrm{e}^{-\delta/\ell_D}, \end{aligned} \quad (4.2)$$

which correspond to well-known formulas of intermolecular forces (Derjaguin 1934; Hamaker 1937), which are independent of the hydrodynamic field or gliding kinematics.

To leading order in η, the Reynolds equation (2.11) becomes

$$r^2\frac{\partial^2 P_0}{\partial r^2} + \left[r + \frac{3r^3}{h_0(r)}\right]\frac{\partial P_0}{\partial r} + \frac{\partial^2 P_0}{\partial\varphi^2} = -\frac{6r^3}{h_0^3(r)}\cos\varphi, \quad (4.3)$$

where P_0 is the leading term of a regular asymptotic expansion of the hydrodynamic pressure in powers of η. Equation (4.3) is subject to boundary conditions (2.12) particularized for the leading-order hydrodynamic pressure. The exact solution

$$P_0 = \left[\frac{\mu U a^{1/2}(1+\omega^2+2\omega\sin\beta)^{1/2}}{\delta^{3/2}}\right]\frac{6r\cos[\theta+\gamma(\omega,\beta)]}{5(1+r^2/2)^2} \quad (4.4)$$

can be obtained in terms of the dimensional hydrodynamic pressure. The contours of (4.4), non-dimensionalized with $\mu U a^{1/2}/\delta^{3/2}$, are shown in figure 4. Note that once the cosine term in (4.4) is expanded, the pressure scaling with the velocity results to be linear in both U and ω, with the total pressure the sum of the pressures induced by each motion mode. The leading-order velocity components can be calculated by using (4.4) and retaining the first term of the expansion in powers of η of (2.13) and (2.14), which yields

$$\left.\begin{aligned} v_{r0} &= \left\{\frac{3z^2(2-3r^2)}{10h_0^3(r)} - \frac{z}{h_0(r)}\left[\frac{3(2-3r^2)}{10h_0(r)}+1\right]\right\}\cos\varphi + \left[\frac{2z}{h_0(r)}-1\right]\frac{\cos(\varphi-\gamma)}{\mathscr{V}(\omega,\beta)}, \\ v_{\varphi 0} &= -\left[\frac{3z^2}{5h_0^2(r)} - \frac{8z}{5h_0(r)}\right]\sin\varphi - \left[\frac{2z}{h_0(r)}-1\right]\frac{\sin(\varphi-\gamma)}{\mathscr{V}(\omega,\beta)}, \\ v_{z0} &= \left[\frac{2z^3(4r-r^3)}{5h_0^4(r)} - \frac{z^2r(r^2+26)}{10h_0^3(r)}\right]\cos\varphi + \frac{z^2r\cos(\varphi-\gamma)}{h_0^2(r)\mathscr{V}(\omega,\beta)}. \end{aligned}\right\} \quad (4.5)$$

Expressions (4.4) and (4.5) reduce to the corresponding pressure and velocity fields in the gap region for the cases of purely translational and rotational motions near a rigid wall (Goldman *et al.* 1967*b*; O'Neill & Stewartson 1967; Cooley & O'Neill 1968).

The calculation of the hydrodynamic drag forces and torques is a singular perturbation problem in the small parameter ϵ, in which it requires asymptotic matching with the outer non-lubrication viscous region. Following earlier work (Goldman *et al.* 1967*b*; O'Neill & Stewartson 1967; Cooley & O'Neill 1968), the

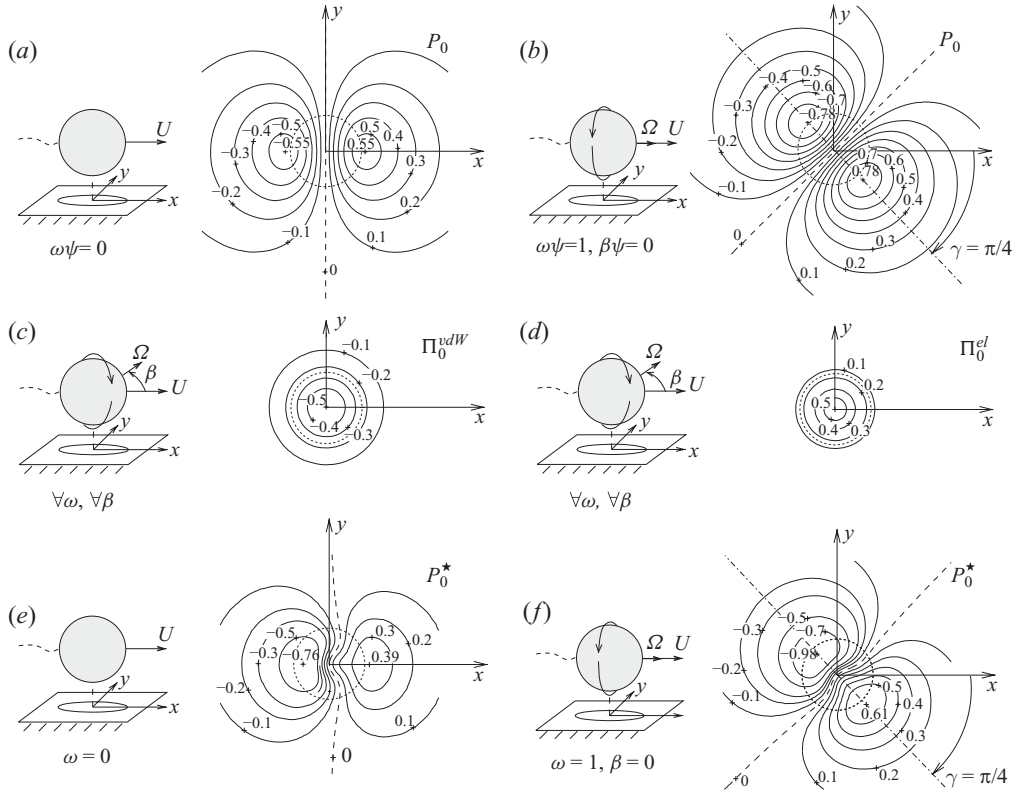

FIGURE 4. Leading-order (rigid-wall) pressure and stress contours. (*a*) Hydrodynamic pressure contours for purely translational motion, (*b*) hydrodynamic pressure contours for corkscrew motion, (*c*) van der Waals stress contours (independent of rotation), (*d*) electric stress contours (independent of rotation), (*e*) hydromolecular pressure contours for purely translational motion and (*f*) hydromolecular pressure contours for corkscrew motion. Positive contour labels represent compression stresses on the substrate, whereas negative ones represent traction stresses. In this figure, $\Upsilon = \Xi = 0.5$, and the dotted line represents a circle of spatial unit radius.

leading-order forces and torques become

$$F^h_{x0} = 6\pi\mu U a\left[\left(\frac{8}{15} - \frac{2}{15}\omega\sin\beta\right)\ln\epsilon - 0.95429 - 0.25725\omega\sin\beta + o(1)\right], \quad (4.6)$$

$$F^h_{y0} = 6\pi\mu\Omega a\cos\beta\left[\frac{2}{15}\ln\epsilon + 0.25725 + o(1)\right], \quad (4.7)$$

$$F^h_{z0} = 0, \quad (4.8)$$

$$T^h_{x0} = 8\pi\mu\Omega a^2\cos\beta\left[\frac{2}{5}\ln\epsilon - 0.37085 + o(1)\right], \quad (4.9)$$

$$T^h_{y0} = 8\pi\mu U a^2\left[\left(\frac{2}{5}\omega\sin\beta - \frac{1}{10}\right)\ln\epsilon - 0.19296 - 0.37085\omega\sin\beta + o(1)\right], \quad (4.10)$$

$$T^h_{z0} = 0, \quad (4.11)$$

which have been conveniently modified in the present investigation to account for an arbitrary azimuth angle of rotation β.

Note that since the problem (2.11) and (2.12) is linear to leading order in η, the hydrodynamic forces (4.6)–(4.11) produced by the rotational and translational motions are decoupled. Because, according to the classical Stokesian scaling, these forces scale linearly with the velocities U and Ω, they are kinematically reversible, in that if the rotation and translation velocity vectors are reversed at once, the forces and torques moduli remain invariant but their directions become reversed. As a result of this kinematically reversible effect, no hydrodynamic lift force is exerted on the sphere to leading order in η, and the intermolecular forces (4.1) and (4.2) are the only forces acting along the normal axis to the substrate. The classic DLVO theory therefore holds in the first approximation, and the particle can only be caused to adhere to the substrate if the electrolyte concentration is larger than its critical coagulation value $c_{i0}^{\triangledown}$ given by (2.23).

Additionally, the decoupling between rotation and translation causes the leading-order drag force (4.6) to remain invariant if rotation about an axis parallel to the translation axis is enabled, $\beta = 0$. This effect is shown in figure 4(a, b) and can be explained in terms of the antisymmetry of the leading-order hydrodynamic pressure with respect to the axis $\theta = \pi/2 - \gamma$ or $\varphi = \pi/2$, for any value of γ, which cancels the effects of the rotational motion on the pressure along the x-axis.

Similarly, a hydrodynamic drift force (4.7) is also exerted on the sphere perpendicularly to its translation axis for $\beta \neq \pi/2$, which solely depends on the rotational velocity. This force can be of paramount importance in the study of the near-contact trajectories of particles and micro-organisms. In particular, the hydrodynamic effect of the drift force in the case of corkscrew motion, $\beta = 0$, was found in an earlier work by Lauga *et al.* (2006), to be responsible, when coupled to the corresponding drift force exerted on its flagella, for the circular swimming-path dynamics of *Escherichia coli* bacteria when they are close to a rigid boundary.

As shown below, effects produced by the presence of a nearby deformable sticky substrate modify the conclusions derived from the rigid-wall case in which (i) a lift force is induced as a result of a combined elastohydromolecular effect, (ii) the forces no longer scale linearly with the velocities, (iii) the drift force becomes dependent on the translational velocity as well, (iv) the drag force does not remain invariant if corkscrew motion is enabled, and (v) the limiting conditions for the onset of adhesion are not generally determined solely by the critical coagulation concentration.

5. Elastohydromolecular forces on a gliding sphere ($\eta > 0$)

The compliance of the substrate couples the hydrodynamic field described by the Reynolds equation (2.11) with the substrate responses (A 19), (A 20) or (A 21), and with the intermolecular stress distributions (2.15) and (2.17). Such coupling effect breaks the intrinsic symmetry of the Stokes equations (2.2)–(2.4) and renders the problems (2.2)–(2.4) and (2.11)–(2.12) nonlinear.

To second order in η, (2.11) becomes

$$r^2\frac{\partial^2 P_1}{\partial r^2} + \left[r + \frac{3r^3}{h_0(r)}\right]\frac{\partial P_1}{\partial r} + \frac{\partial^2 P_1}{\partial \varphi^2} = \frac{18}{5}\frac{r^3(6+r^2)}{h_0^5(r)}H_0\cos\varphi + \frac{48}{5}\frac{r}{h_0^3(r)}\frac{\partial H_0}{\partial \varphi}\sin\varphi + \frac{12}{5}\frac{r^2(r^2-4)}{h_0^4(r)}\frac{\partial H_0}{\partial r}\cos\varphi. \quad (5.1)$$

Equation (5.1) is subject to boundary conditions (2.12). The case of a thin compressible layer (A 19) is addressed in detail in this section.

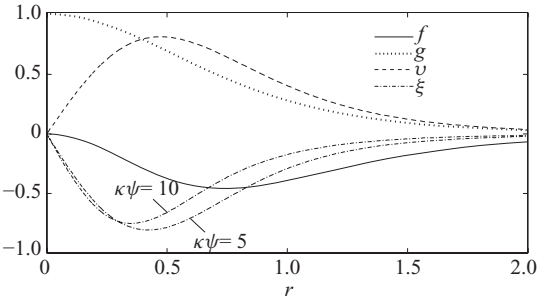

FIGURE 5. Functions f, g, υ and ξ obtained from the numerical integration of (5.5)–(5.8).

To leading order in η, (A 19) yields the normal surface deformation

$$H_0 = P_0 + \Pi_0^{vdW} + \Pi_0^{el} = \frac{6r\cos\varphi}{5h_0^2(r)} - \frac{\Upsilon}{h_0^3(r)} + \Xi \mathrm{e}^{-\kappa[h_0(r)-1]}. \tag{5.2}$$

Substituting this expression into the second-order balance Reynolds equation (5.1), we obtain

$$r^2\frac{\partial^2 P_1}{\partial r^2} + \left[r + \frac{3r^3}{h_0(r)}\right]\frac{\partial P_1}{\partial r} + \frac{\partial^2 P_1}{\partial \varphi^2} = \frac{72}{25}\frac{r^4(20+r^2)}{h_0^7(r)}\cos^2\varphi + \left\{\frac{18}{5}\frac{\Upsilon r^3(r^2-14)}{h_0^8(r)} + \frac{12}{5}\frac{\Xi\kappa r^3(4-r^2)\mathrm{e}^{-\kappa[h_0(r)-1]}}{h_0^4(r)} + \frac{18}{5}\frac{\Xi r^3(6+r^2)\mathrm{e}^{-\kappa[h_0(r)-1]}}{h_0^5(r)}\right\}\cos\varphi - \frac{288}{25}\frac{r^2}{h_0^5(r)}. \tag{5.3}$$

A particular integral of the form

$$P_1 = f(r)\cos^2\varphi + [\Upsilon\upsilon(r) + \Xi\xi(r,\kappa)]\cos\varphi + g(r) \tag{5.4}$$

is substituted into (5.3), which yields the linear system of ordinary differential equations

$$\mathscr{L}_2 f = \frac{72}{25}\frac{r^4(20+r^2)}{h_0^7(r)}, \tag{5.5}$$

$$\mathscr{L}_1\upsilon = \frac{18}{5}\frac{r^3(r^2-14)}{h_0^8(r)}, \tag{5.6}$$

$$\mathscr{L}_1\xi = \frac{12}{5}\frac{\kappa r^3(4-r^2)\mathrm{e}^{-\kappa[h_0(r)-1]}}{h_0^4(r)} + \frac{18}{5}\frac{r^3(6+r^2)\mathrm{e}^{-\kappa[h_0(r)-1]}}{h_0^5(r)}, \tag{5.7}$$

$$\mathscr{L}_0 g + 2f = -\frac{288}{25}\frac{r^2}{h_0^5(r)}, \tag{5.8}$$

with $\mathscr{L}_n$ a differential operator given by

$$\mathscr{L}_n = r^2\frac{\mathrm{d}^2}{\mathrm{d}r^2} + \left[r + \frac{3r^3}{h_0(r)}\right]\frac{\mathrm{d}}{\mathrm{d}r} - n^2, \quad \text{with} \quad n = 0, 1, 2. \tag{5.9}$$

For $r \ll 1$, $f = O(r^2)$, $g = O(1)$, $\upsilon = O(r)$ and $\xi = O(r)$. Similarly, for $r \gg 1$, $f = O(r^{-8})$, $g = O(r^{-8})$, $\upsilon = O(r^{-11})$ and $\xi = O(\mathrm{e}^{-\kappa r^2}/r^3)$. Therefore, the boundary conditions of (5.5)–(5.8) are $f = \upsilon = \xi = 0$ and $g' = 0$ for $r = 0$, and vanishing values of f, g, υ and ξ for large r. Figure 5 shows the solutions to (5.5)–(5.8), which need to be obtained numerically. Nonetheless, for later use, the auxiliary function $\sigma = 2g + f$

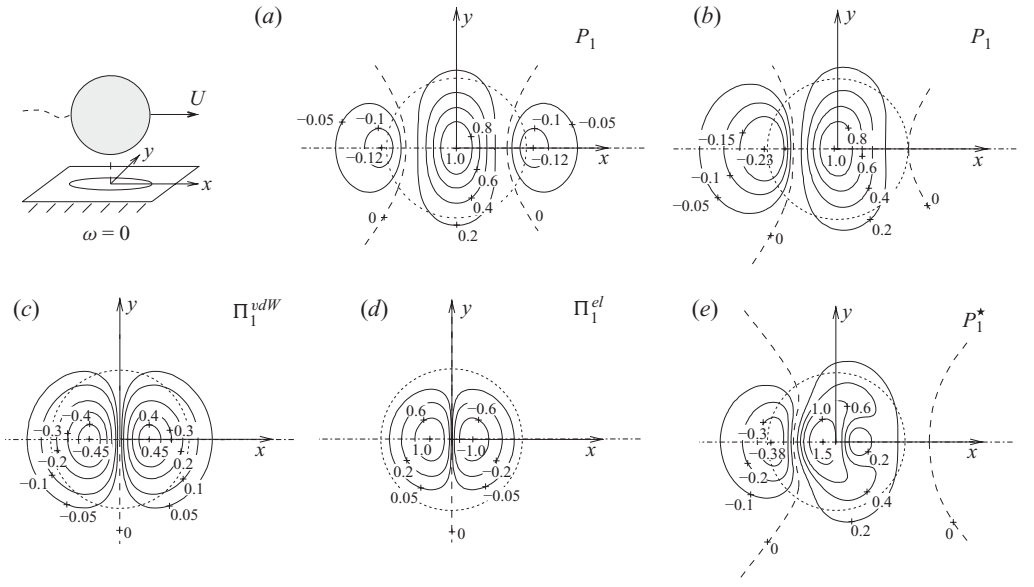

FIGURE 6. Second-order pressure and stress contours for purely translational motion. (*a*) The hydrodynamic pressure disturbance in the absence of intermolecular effects, $\Xi = \Upsilon = 0$, and the influences of intermolecular effects, with $\Xi = \Upsilon = 0.5$, on (*b*) the hydrodynamic pressure, (*c*) van der Waals stress, (*d*) electric stress and (*e*) hydromolecular pressure perturbations. The dotted line represents a circle of spatial unit radius.

is defined by combining (5.5) and (5.8). It can be shown that the resulting differential equation has the exact solution

$$\sigma = 2g + f = \frac{18}{125}\frac{(14 - 5r^2)}{h_0^5(r)}, \quad \text{with} \quad \int_0^\infty \sigma r \, \mathrm{d}r = \frac{48}{125}. \tag{5.10}$$

The dimensionless hydromolecular pressure perturbation is given by

$$\begin{aligned} P_1^\star &= P_1 + \Pi_1^{vdW} + \Pi_1^{el} \\ &= f(r)\cos^2\varphi + \left\{ \Upsilon \left[\upsilon(r) + \frac{18r}{5h_0^6(r)} \right] + \Xi \left[\xi(r,\kappa) - \frac{6r\kappa \mathrm{e}^{-\kappa[h_0(r)-1]}}{5h_0^2(r)} \right] \right\} \cos\varphi \\ &\quad + g(r) - \frac{3\Upsilon^2}{h_0^7(r)} - \kappa \Xi^2 \mathrm{e}^{-2\kappa[h_0(r)-1]} + \Xi\Upsilon \left\{ \frac{\mathrm{e}^{-\kappa[h_0(r)-1]}}{h_0^3(r)} \left[\frac{3}{h_0(r)} + \kappa \right] \right\}, \end{aligned} \tag{5.11}$$

where we use (3.2), (3.3), (5.2) and (5.4). Because $P_1^\star$ decays sufficiently rapidly for large r, the calculation of the force and torque perturbations thereby is not a singular perturbation problem, in which the required indefinite integrals of the hydromolecular pressure perturbation are convergent for large r.

Figures 6 and 7 show the contours of the first perturbations of the hydrodynamic pressure (5.4), the hydromolecular pressure (5.11) and the intermolecular stresses (3.2) and (3.3), non-dimensionalized with $\mu U a^{1/2}/\delta^{3/2}$, to illustrate the rotational effects. The substrate compliance decreases and increases the hydrodynamic overpressure and underpressure levels respectively, which breaks the antisymmetry of the leading-order hydrodynamic pressure contours and induces a lift force, and drag-force and drift-force perturbations. Note that the corkscrew rotation actively affects the pressure

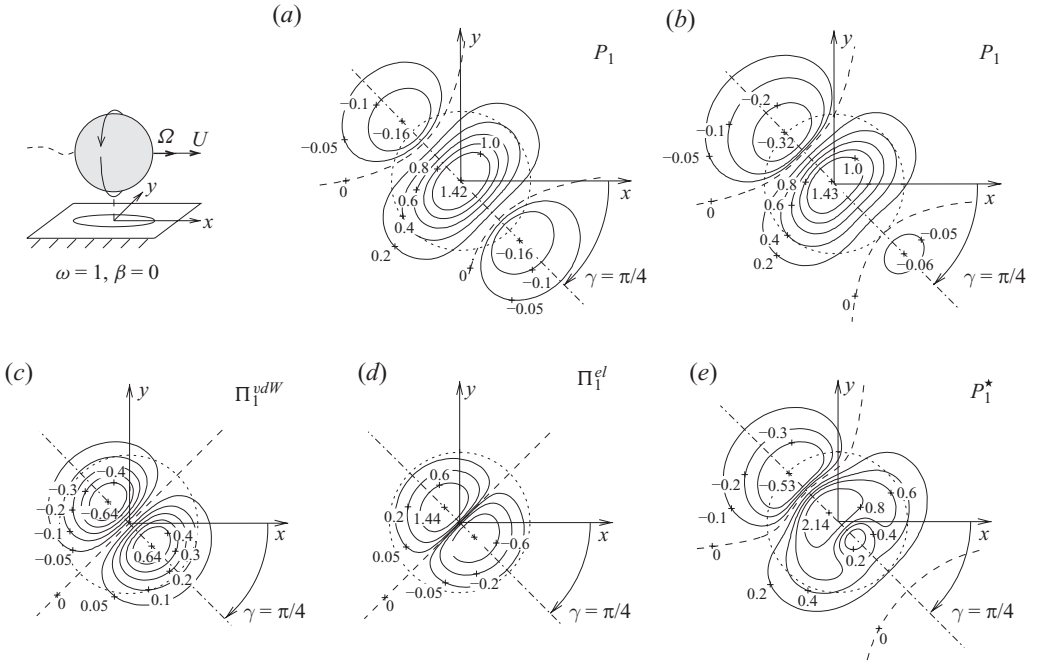

FIGURE 7. Second-order pressure and stress contours for corkscrew motion. (*a*) The hydrodynamic pressure disturbance in the absence of intermolecular effects, $\Xi = \Upsilon = 0$, and the influences of intermolecular effects, with $\Xi = \Upsilon = 0.5$, on (*b*) the hydrodynamic pressure, (*c*) van der Waals stress, (*d*) electric stress and (*e*) hydromolecular pressure perturbations. The dotted line represents a circle of spatial unit radius.

component of the drag force, as observed by comparing the projection along the x-axis of the contours in figures 6 and 7 and superposing them onto those shown in figure 4.

The shear-stress perturbations can be obtained by differentiating the second term of the expansion of (2.13) and (2.14) in powers of η_0, which yields

$$\tau_{rz1} = \left.\frac{\partial v_{r1}}{\partial z}\right|_{z=h_0(r)} = \left[\frac{12r(4-r^2)}{25h_0^5(r)} + \frac{h_0(r)}{2}\frac{\mathrm{d}f(r)}{\mathrm{d}r}\right]\cos^2\varphi + \left\{\frac{\Upsilon}{h_0^5(r)} - \frac{\Xi \mathrm{e}^{-\kappa[h_0(r)-1]}}{h_0^2(r)}\right\}\frac{2\cos(\varphi-\gamma)}{\mathscr{V}(\omega,\beta)} + \left\{\frac{2\Xi(4-r^2)\mathrm{e}^{-\kappa[h_0(r)-1]}}{5h_0^3(r)} + \frac{2\Upsilon(r^2-4)}{5h_0^6(r)} + \frac{h_0(r)}{2}\left[\Upsilon\frac{\mathrm{d}\upsilon(r)}{\mathrm{d}r} + \Xi\frac{\partial\xi(r,\kappa)}{\partial r}\right]\right\}\cos\varphi - \frac{12r\cos\varphi\cos(\varphi-\gamma)}{5h_0^4(r)\mathscr{V}(\omega,\beta)} + \frac{h_0(r)}{2}\frac{\mathrm{d}g(r)}{\mathrm{d}r}, \tag{5.12}$$

and

$$\tau_{\varphi z1} = \left.\frac{\partial v_{\theta 1}}{\partial z}\right|_{z=h_0(r)} = -\left[\frac{48r}{25h_0^4(r)} + \frac{h_0(r)f(r)}{r}\right]\sin\varphi\cos\varphi + \left\{\frac{8\Upsilon}{5h_0^5(r)} - \frac{8\Xi\mathrm{e}^{-\kappa[h_0(r)-1]}}{5h_0^2(r)} - \frac{[\Upsilon\upsilon(r)+\Xi\xi(r,\kappa)]h_0(r)}{2r}\right\}\sin\varphi + \left[\frac{\Xi\mathrm{e}^{-\kappa[h_0(r)-1]}}{h_0^2(r)} - \frac{\Upsilon}{h_0^5(r)}\right]\frac{2\sin(\varphi-\gamma)}{\mathscr{V}(\omega,\beta)} + \frac{12r\cos\varphi\sin(\varphi-\gamma)}{5h_0^4(r)\mathscr{V}(\omega,\beta)}, \tag{5.13}$$

where we use (5.2) and (5.4).

The values of the forces obtained from the analytical integration of (5.11)–(5.13) are compared in what follows to the numerical solution of the problem (2.11), (2.12) and (A 19), which was integrated by using a second-order finite-differences numerical scheme. In this investigation, torques are not calculated since they are found to be of $O(\epsilon\eta_0)$, which correspond to higher-order effects that are not considered here.

5.1. *Lift force*

Integrating the asymptotic expansion of the hydromolecular pressure (5.11) over the vertical projection of the inner element of the surface of the sphere in cylindrical coordinates, $\mathrm{d}S_z = -a^2\epsilon r\,\mathrm{d}r\,\mathrm{d}\varphi\boldsymbol{e}_z$, and using expressions (5.10), the elastohydromolecular lift force

$$\begin{aligned} F_z &= \frac{\mu U \mathscr{V}(\omega,\beta)a}{\epsilon^{1/2}} \int_0^{\infty}\int_0^{2\pi} P_1^{\bigstar} r\,\mathrm{d}r\,\mathrm{d}\varphi \\ &= \frac{\pi\mu U \mathscr{V}(\omega,\beta)a}{\epsilon^{1/2}} \left\{ -\Upsilon + \frac{2\Xi}{\kappa} + \eta_0\left[\frac{48}{125} - (\Upsilon-\Xi)^2\right] \right. \\ &\quad \left. + O\left(\eta_0^3, \eta_0^3\Upsilon^2, \eta_0^3\Xi^2, \eta_0^3\Upsilon\Xi, \eta_0^3\Upsilon^2\Xi^2, \eta_0^3\Upsilon\Xi^3, \eta_0^3\Upsilon^3\Xi\right) \right\} \end{aligned} \tag{5.14}$$

is obtained. It can be shown that the contribution of the shear stresses to the lift force is of order $\epsilon\eta_0 \ll \eta_0$ (Urzay *et al.* 2007), which is neglected in this analysis. The lift force (5.14) is composed of two leading-order terms that represent the values (4.1) and (4.2) of the intermolecular forces on a small sphere near a rigid wall. These are the two fundamental acting forces in the DLVO theory. The lift force also includes a term $48\eta_0/125$, which corresponds to the positive elastohydrodynamic lift force (Weekley *et al.* 2006; Urzay *et al.* 2007). The term $-(\Upsilon-\Xi)^2$ in the squared bracket represents a negative elastomolecular lift force that is a nonlinear superposition of intermolecular effects; this force corresponds to the disturbance of the intermolecular force on a stationary sphere induced by the soft substrate, as shown in Appendix B by the second-order term of (B 2). Higher-order terms result from a full elastohydromolecular coupling and involve combinations of the hydrodynamic and intermolecular compliances, such that the resulting dimensionless groups are proportional to even powers of the velocity; the expansion of the lift force remains kinematically irreversible to every order, in which its direction is independent of the direction of rotation and translation.

To leading order in η_0, only the DLVO force, the origin of which is purely related to the intermolecular stresses and not hydrodynamically enhanced, acts on the particle along the z-axis; this force is kinematically irreversible, although the flow is still Stokesian in a linear sense. For non-zero η_0, the existence of a kinematically irreversible lift force of elastohydromolecular origin is explained in terms of the nonlinearity induced by the substrate compliance and intermolecular effects. Nonlinear effects in Stokes-type flows can be produced by small convective disturbances in the flow (Saffman 1964; Leighton & Acrivos 1985), non-Newtonian fluid behaviours (Hu & Joseph 1999) or electrokinetic effects (Bike & Prieve 1995), all of which induce kinematically irreversible forces on submerged particles and are important in certain range of rheological applications. In this model, the elastohydromolecular lift force is produced by the combined action of the intermolecular and hydrodynamic stresses on the substrate, which ultimately modify the compliant gap geometry and

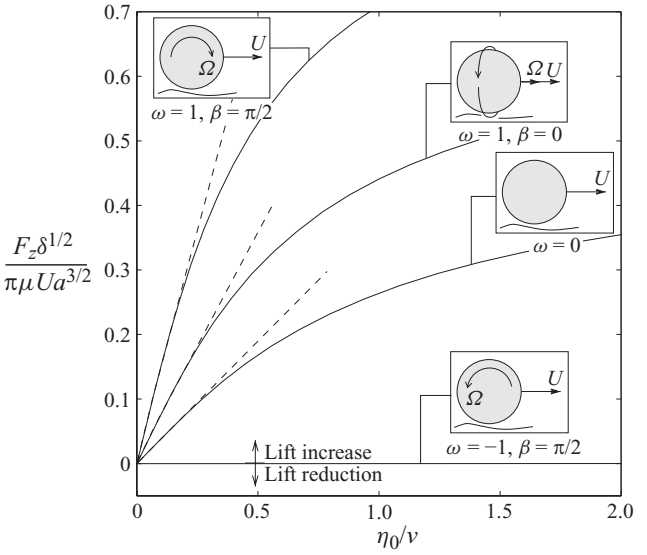

FIGURE 8. Influences of rotation ω and azimuth angle of rotation β on the lift force (5.14) in the absence of intermolecular forces, $\Xi = \Upsilon = 0$. The numerical and asymptotic solutions are shown by solid and dashed lines, respectively.

the hydrodynamic flow through that region as shown by the contours of the pressure and stress disturbances in figures 6 and 7.

5.1.1. *Influences of rotation and of rotation-axis orientation on the lift force*

Rotational motions distort the magnitude and orientation of the pressure distribution in the gap and also modify the gap geometry, as observed in figure 7. To isolate the rotational effects, the lift force (5.14) is non-dimensionalized independently of the velocity scale $\mathscr{V}(\omega, \beta)$, and expressed as a function of the translational hydrodynamic compliance $\eta_0/\mathscr{V}(\omega, \beta)$ as shown in figure 8, where intermolecular effects have been neglected for illustrative purposes. As advanced in a previous study (Urzay *et al.* 2007), the inverse purely rolling motion ($\omega = -1$, $\beta = \pi/2$) completely suppresses the production of elastohydrodynamic lift force, since a local Couette flow is induced in the gap, and the hydrodynamic pressure becomes zero to every order of η_0. That is not the case when the intermolecular forces are not negligible, since both the leading-order intermolecular and second-order elastomolecular contributions to the lift force are present in (5.14). Similarly, the present formulation reveals that, for the same translational velocity, particle dimensions and substrate mechanical properties, the purely rolling motion ($\omega = 1$, $\beta = \pi/2$) produces a larger lift force than the corkscrew ($\omega = 1$, $\beta = 0$) and translational ($\omega = 0$) motions; during the rolling motion, the fluid entrainment of the combined rotation and translation are aligned along the $\theta = 0$ axis and both effects more strongly synergize causing a larger positive overpressure peak in the gap and therefore larger substrate deformations. In this model, no negative values of the elastohydrodynamic lift force were found for any combination of rotation and translation.

5.1.2. *Influences of intermolecular effects on the lift force*

Figure 7 shows that the intermolecular stresses produced by the electric and van der Waals forces disturb the compliant wall and modify the net normal stress acting on

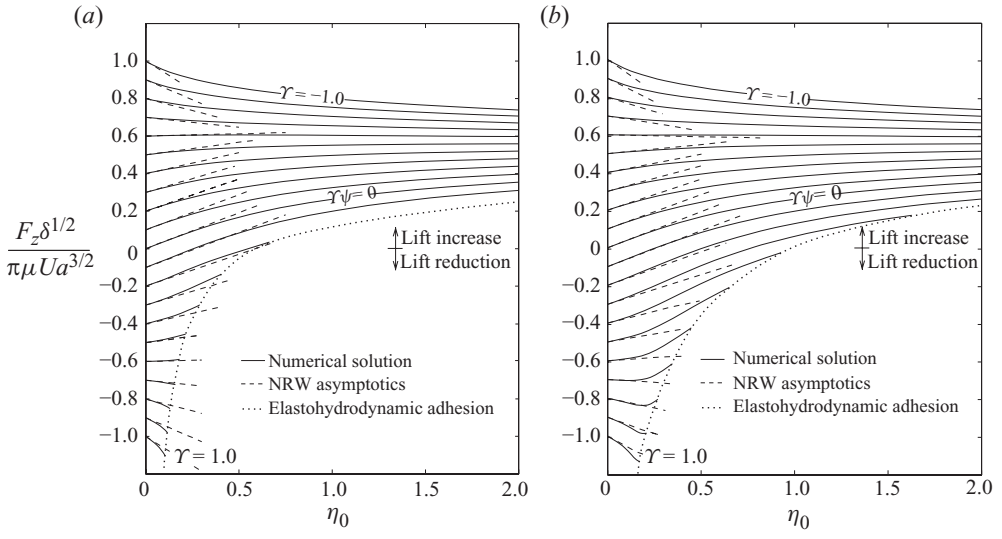

FIGURE 9. Dimensionless elastohydromolecular lift force on the sphere, for any rotation rate and rotation axis orientation, as a function of the hydrodynamic compliance η_0 for $-1 \leqslant \Upsilon \leqslant 1$, with an interval step $\Delta\Upsilon = 0.1$ between lines, for (a) deionized solvents, $\Xi = 0$, and (b) ionized solvents with $\Xi = 0.035$ (electric repulsion) and $\kappa = 10$. The dotted envelope line represents the values for elastohydrodynamic adhesion, beyond which no solution of (2.11), (2.12) and (A 19) was found because of a loss of static mechanical equilibrium on the substrate surface.

the sphere. The influences of these intermolecular effects on the lift force are shown in figure 9, which values are independent of ω and β. For negative and order-unity values of Υ, or more precisely $\Upsilon \lesssim -(48/125)^{1/2}$, which correspond to order-unity and repulsive van der Waals forces, the lift force decreases with increasing η_0 because of the gap-distance-augmentation effect outlined in Appendix B, by which the repulsion decreases because of the increase of the substrate compliance and the effective clearance, which dominates the elastohydrodynamic force that typically increases with increasing η_0. For smaller but repulsive van der Waals forces, $-(48/125)^{1/2} \lesssim \Upsilon < 0$, the lift force is positive and increases with η_0. Slightly attractive van der Waals forces produce negative lift forces on the sphere up to a resuspension or lift-off hydrodynamic compliance η_{0L}, beyond which the elastohydrodynamic effect dominates and a positive lift force occurs. This increase proceeds up to a critical hydrodynamic compliance η_{0C} for the occurrence of irreversible elastohydrodynamic adhesion, in which no solution of the problem (2.11), (2.12) and (A 19) is found beyond η_{0C} at constant Υ because of a loss of static mechanical equilibrium on the substrate surface. Positive and order-unity values of Υ, which correspond to large and attractive van der Waals forces, enhance earlier irreversible elastohydrodynamic adhesion. The lift-off and elastohydrodynamic adhesion processes are addressed in detail in § 6, and a similar but simpler adhesion phenomenon is exemplified in Appendix B for a stationary sphere. Solvent ionization and electric repulsion augment the lift force, decrease the magnitude of the lift-off hydrodynamic compliance, and they extend the irreversible elastohydrodynamic adhesion boundary to larger η_{0C} by electrically stabilizing the substrate surface.

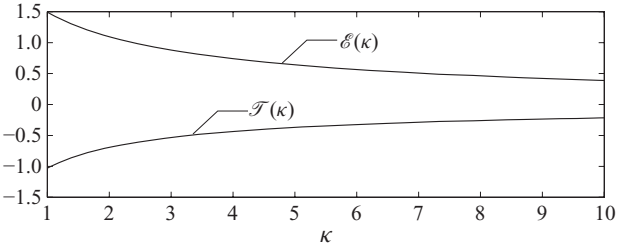

FIGURE 10. Drag and drift coefficients (5.17) of the electric force.

5.2. *Drag-force and drift-force first perturbations*

The perturbations of the drag and drift forces on the sphere are calculated as

$$\begin{aligned} F_{x1} &= -\mu U \mathscr{V} a \eta_0 \int_0^{2\pi}\int_0^{\infty} \left[P_1^{\bigstar} r^2 \cos(\varphi-\gamma) + \tau_{rz1} r \cos(\varphi-\gamma) - \tau_{\varphi z1} r \sin(\varphi-\gamma)\right] \mathrm{d}r\, \mathrm{d}\varphi \\ &= \pi\mu U a \eta_0 \big\{ \Xi\left[\mathscr{E}(\kappa) + \mathscr{J}(\kappa)\omega \sin\beta\right] - \Upsilon\left[\mathscr{F} - \mathscr{G}\omega\sin\beta\right] \\ &\quad + O\big(\eta_0^2, \eta_0\Upsilon^2, \eta_0\Xi^2, \eta_0\Xi\Upsilon\big)\big\}, \end{aligned} \tag{5.15}$$

and

$$\begin{aligned} F_{y1} &= -\mu U \mathscr{V} a \eta_0 \int_0^{2\pi}\int_0^{\infty} \left[P_1^{\bigstar} r^2 \sin(\varphi-\gamma) + \tau_{rz1} r \sin(\varphi-\gamma) + \tau_{\varphi z1} r \cos(\varphi-\gamma)\right] \mathrm{d}r\, \mathrm{d}\varphi \\ &= -\pi\mu U a \eta_0 \Big\{ \omega\cos\beta\left[\Upsilon\mathscr{G} + \Xi\mathscr{J}(\kappa)\right] + O\big(\eta_0^2, \eta_0\Upsilon^2, \eta_0\Xi^2, \eta_0\Xi\Upsilon\big)\Big\} \end{aligned} \tag{5.16}$$

where the electric force coefficients $\mathscr{E}(\kappa)$ and $\mathscr{J}(\kappa)$ are given by

$$\left.\begin{aligned} \mathscr{E}(\kappa) &= 2 - \frac{6\kappa}{5} + (6\kappa - 4)\frac{\kappa}{5}\mathrm{e}^{\kappa}\mathrm{Ei}(-\kappa) - \frac{1}{2}\int_0^{\infty} \xi(r,\kappa) r^2\, \mathrm{d}r, \\ \mathscr{J}(\kappa) &= -2 - \frac{6\kappa}{5} - \frac{\kappa}{5}(6\kappa + 16)\mathrm{e}^{\kappa}\mathrm{Ei}(-\kappa) + \frac{1}{2}\int_0^{\infty} \xi(r,\kappa) r^2\, \mathrm{d}r, \end{aligned}\right\} \tag{5.17}$$

which are shown in figure 10, and with the van der Waals force coefficients $\mathscr{F}$ and $\mathscr{G}$ given by

$$\mathscr{F} = \frac{17}{25} + \frac{1}{2}\int_0^{\infty} \upsilon(r) r^2\, \mathrm{d}r = 0.9905 \quad \text{and} \quad \mathscr{G} = \frac{8}{25} - \frac{1}{2}\int_0^{\infty} \upsilon(r) r^2\, \mathrm{d}r = 0.0095. \tag{5.18}$$

The drag-force and drift-force perturbations are composed of two terms of $O(\eta_0\Upsilon)$ and $O(\eta_0\Xi)$: the van der Waals and electric drag/drift forces. These are representative of the forces induced by mixed elastohydromolecular effects. Higher-order terms involve combinations of the hydrodynamic and intermolecular compliances, such that the resulting dimensionless groups are proportional to odd powers of the velocity; the expansions of the drag and drift force remain kinematically reversible to every order, in which their direction changes under gliding direction reversal. Note that if the intermolecular effects are negligible, $\Upsilon = \Xi = 0$, the substrate-deformation effects on the drag and drift forces become of $O(\eta_0^2)$ for $\eta_0 \ll 1$, which cannot be analytically captured by solely retaining the order $O(\eta_0)$ terms in the expansions (5.15) and (5.16).

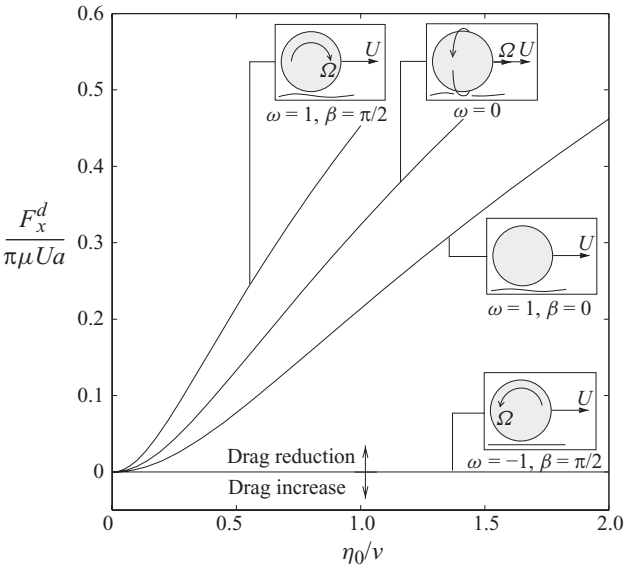

FIGURE 11. Influences of rotation ω and azimuth angle of rotation β on the drag-force disturbance, obtained by numerical integration of (2.11), (2.12) and (A 19), in the absence of intermolecular forces, $\Upsilon = \Xi = 0$.

5.2.1. *Influences of rotation and rotation-axis orientation on the drag-force disturbance*

Figure 11 shows the effects of the rotation ω and the azimuthal orientation β of the rotation axis on the disturbance of the drag force, obtained by numerical integration of (2.11), (2.12) and (A 19), in the absence of intermolecular forces, $\Upsilon = \Xi = 0$. The substrate compliance reduces the leading-order drag force (4.6) because of a decrease in the hydromolecular pressure and viscous shear stresses in the deformed gap region. The inverse purely rolling motion ($\omega = -1$, $\beta = \pi/2$) completely suppresses the elastohydrodynamic drag-force disturbance, since no deformation is produced in this case. For the same translational velocity, particle dimensions and substrate mechanical properties, the purely rolling motion ($\omega = 1$, $\beta = \pi/2$) produces a larger drag-force reduction than the corkscrew ($\omega = 1$, $\beta = 0$) and translational ($\omega = 0$) motions. For $\eta_0 = O(1)$, the elastohydrodynamic drag-force disturbance produced by surface-deformation effects is approximately $6\ln(1/\epsilon)$ times smaller than the leading-order force (4.6), which, as a maximum, represents a 5 %–10 % drag reduction for $\epsilon = 0.1$. It must be emphasized that the rotational and translational motions are nonlinearly coupled as in the corkscrew motion, for which rotation about an axis parallel to the translation axis induces an additional drag reduction; this nonlinear effect departs from the decoupled behaviour of the rotational and translational motions observed in the leading-order drag force (4.6), which is typical of linear viscous flows. In this model, no negative values of the elastohydrodynamic drag-force disturbance were found for any combination of rotation and translation.

5.2.2. *Influences of the intermolecular effects on the drag-force disturbance*

The influences of the intermolecular effects on the drag-force disturbance on the sphere are shown in figure 12. For negative values of Υ, which correspond to repulsive

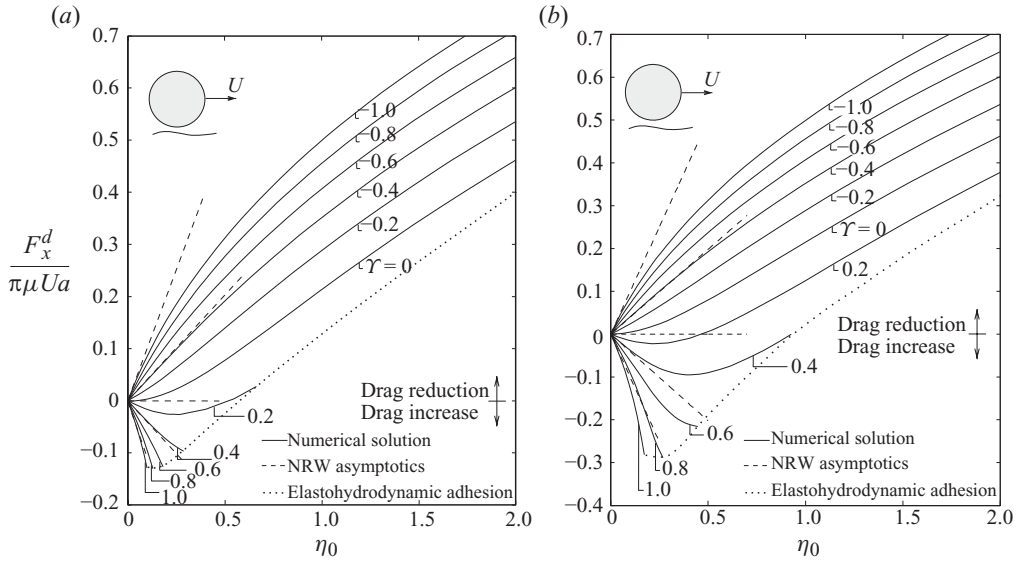

FIGURE 12. Dimensionless elastohydromolecular drag-force disturbance on a translating sphere as a function of the hydrodynamic compliance η_0 for $-1 \leqslant \Upsilon \leqslant 1$, for ($a$) deionized solvents, $\Xi = 0$, and (b) ionized solvents with $\Xi = 0.035$ (electric repulsion) and $\kappa = 10$. The dotted envelope line represents the values for hydrodynamic adhesion, beyond which no numerical solution of (2.11), (2.12) and (A 19) was found because of a loss of static mechanical equilibrium on the substrate surface.

van der Waals forces, the drag-force disturbance increases with η_0, which results in an additional drag reduction to that solely produced by substrate-deformation effects. Slightly attractive van der Waals forces, $\Upsilon \ll 1$, produce a drag increase on the sphere up to a critical compliance, beyond which the elastohydrodynamic effect dominates and a drag reduction occurs. Positive and order-unity values of Υ, which correspond to large and attractive van der Waals forces enhance irreversible elastohydrodynamic adhesion. Electric repulsion augments the drag-reduction trend and extends the elastohydrodynamic adhesion boundary to larger η_0.

5.2.3. *Influences of the intermolecular effects on the drift-force disturbance*

Substrate-deformation effects are found to play a very weak role on the drift force. For a stationary rotating sphere near a soft substrate, $\omega \to \infty$, $U \to 0$, this can be explained in terms of the mutual cancellation of the two following effects: a hydrodynamic overpressure decrease in the gap region, which increases the drift, and the loss of traction due to the viscous shear-stress decrease in the same region, which reduces the drift force; both effects are found to be of the same magnitude in the range of hydrodynamic compliances η_0 studied in this analysis, which yields a negligibly small drift disturbances with respect to the leading-order force (4.7). Nonetheless, (5.16) predicts a drift reduction and increase due to electric repulsion and van der Waals forces, respectively, both of which actively modify the shear stress distribution in the gap and the viscous-traction efficiency.

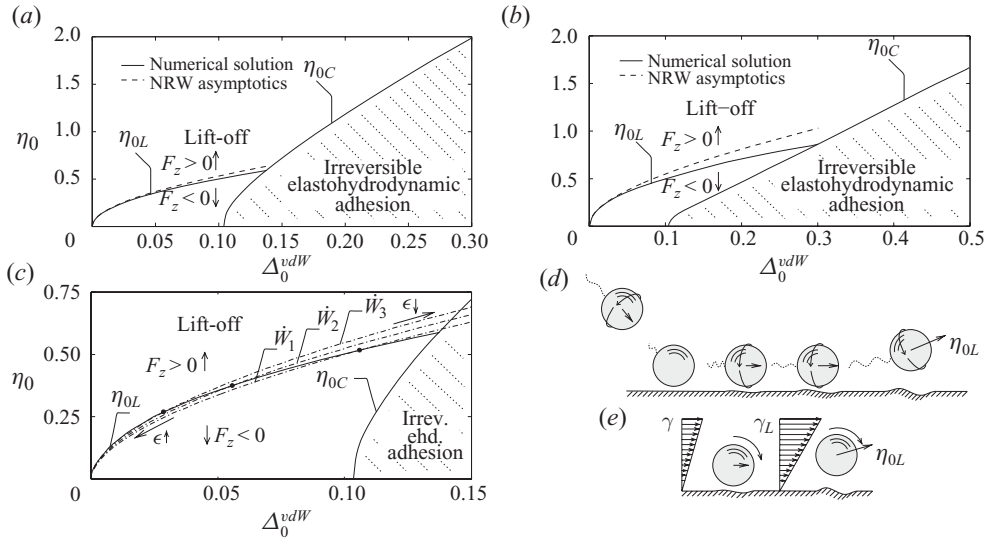

FIGURE 13. Lift-off and critical hydrodynamic compliances for elastohydrodynamic adhesion as a function of the van der Waals compliance, for (*a*) deionized solvents, $\Xi = 0$, and (*b*) ionized solvents with $\Xi = 0.035$ (electric repulsion) and $\kappa = 10$. (*c*) Gliding-power $\dot{W}$ isolines (dot-dashed lines) in deionized solvents, with $\dot{W}_1 < \dot{W}_2 < \dot{W}_3$. The figure also shows two examples of migration mechanisms on a soft and sticky substrate. (*d*) Swimming-induced migration: a slow swimmer gets entrapped in an accessible potential minimum as it approaches the substrate surface, from where it escapes when the lift-off velocity η_L is achieved. (*e*) Shear-induced migration: a particle close to the substrate migrates under the action of sufficiently high shear rates γ_L.

6. Elastohydrodynamic adhesion and lift-off

A characteristic lift-off compliance η_{0L} can be defined as that for which the lift force becomes zero:

$$\eta_{0L} \approx \left\{ \frac{125}{48} \left[\Delta_0^{vdW} - \frac{2\Delta_0^{el}}{\kappa} + \left(\Delta_0^{vdW} - \Delta_0^{el} \right)^2 \right] \right\}^{1/2}, \tag{6.1}$$

which is representative of the reversible adhesion on the substrate; for $\eta_0 = \eta_{0L}$, the particle can undergo lateral motions along the substrate surface. For a given set of intermolecular parameters and particle dimensions, the lift-off hydrodynamic compliance can be achieved by sufficiently large gliding velocities or substrate compliances.

For $\eta_0 < \eta_{0L}$, the lift force on the particle is negative, and irreversible elastohydrodynamic adhesion occurs for sufficiently large Δ_0^{vdW}. This adhesion mechanism is due to surface instabilities on the substrate, and however qualitatively similar to the elastostatic adhesion mechanism for a stationary sphere presented in Appendix B; here the hydrodynamic pressure plays an important role in the stabilization of the surface. The limiting values for irreversible elastohydrodynamic adhesion are given by the critical hydrodynamic compliance η_{0C}, which needs to be calculated numerically and depends on the intermolecular compliances as shown in figure 13(*a*, *b*). For $\eta_0 > \eta_{0L}$, the lift force is positive, but irreversible elastohydrodynamic adhesion is not fully prevented since the substrate becomes softer and more unstable as η_0 increases.

That adhesion can occur for positive lift forces may represent a counter-intuitive event, especially if comparison to the stationary-sphere case in Appendix B is made, because elastostatic adhesion always occurs there for net attractive intermolecular forces. This concept can be explained by use of figure 9 where, by holding Υ and Ξ constant and varying η_0, effects induced solely by the substrate softness can be extracted: irreversible elastohydrodynamic adhesion events for $F_z > 0$ observed in figure 9 show that sufficiently large compliances destabilize the substrate surface for a given gliding velocity, particle dimensions, gap distance and intermolecular intensity, and promote adhesion by decreasing the strength of the restoring elastic stress. Similarly, effects induced solely by the gliding velocity can be extracted by keeping Δ_0^{vdW} constant in figure 13(*a*, *b*) and varying η_0 along a vertical line: sufficiently small gliding velocities enhance elastohydrodynamic adhesion by hydrodynamically destabilizing the substrate surface for a given substrate compliance, gap distance, particle dimensions and intermolecular intensity. An increase on the repulsive electric force decreases the extension of the hydrodynamic adhesion region, as shown in figure 13(*b*), by exerting a stabilizing compressive stress on the substrate surface. The irreversible elastohydrodynamic adhesion mechanism can occur in ionized and deionized solvents. In deionized solvents there is no spontaneous electrical interaction; therefore elastohydrodynamic adhesion cannot be described by the classic DLVO theory.

It is worth emphasizing that the reversible elastohydrodynamic regime $\eta_0 = \eta_{0L}$ corresponds to a stable regime in a dynamic lift-off process at constant gliding power $\dot{W}$ under small quasi-static perturbations of the gap distance. An iso-power gliding trajectory $\dot{W} = F_{x0}U = \text{constant}$, on a $\{\eta_0, \Delta_0^{vdW}\}$ plane, is given by

$$\eta_0 \sim C_1 \Delta_0^{vdW^{5/8}} \left[\ln(\Delta_0^{vdW^{1/4}}/C_2) \right]^{-1/2} \tag{6.2}$$

for deionized solvents, where $C_1 = f(\dot{W}) = O(1)$ and $C_2 = O(\epsilon \Delta_0^{vdW^{1/4}}) = O(\Delta_{0a}^{vdW^{1/4}}) \ll 1$ are two constants, with $\Delta_{0a}^{vdW^{1/4}}$ as the van der Waals compliance based on a gap distance of $O(a)$. A necessary requirement for (6.2) to be accurate is that $\Delta_0^{vdW^{1/4}} \gg C_2$, since $\epsilon = O(1)$ when $\Delta_0^{vdW^{1/4}} = O(C_2)$. As shown in figure 13(*c*), a small decrease of the minimum gap clearance δ below its lift-off value induces a positive lift force, which returns the particle to its initial vertical position above the substrate. However, a sufficiently large perturbation of the particle position towards the substrate can induce irreversible elastohydrodynamic adhesion. Similarly, an increase of the minimum gap clearance above its lift-off value induces a positive lift force, which returns the particle to its initial vertical position above the substrate. This stable equilibrium is similar to that found for ionized solvents in the DLVO secondary minimum, from which particles and micro-organisms are believed to be able to escape from the potential well due to van der Waals retardation effects at large gap distances (Israelachvili 1985; Lyklema 2005). Similar dynamics are found for constant-force trajectories. On the basis of these results, a reversible adhesion regime and resuspension may be envisioned for a constant-power micro-swimmer as that depicted in figure 13(*d*). The lift-off and lateral motility of the swimmer are entirely elastohydrodynamically enhanced, such that these effects cease to exist once the gliding motion stops.

Similar phenomena have been observed in the slip and flow of dense polymer microgel pastes in earlier works (Meeker *et al.* 2004; Seth *et al.* 2008), where experiments, scaling and numerical analyses of elastohydrodynamic models found a slip regime of sheared pastes over surfaces beyond a critical sliding yield stress. Below the sliding yield stress, the paste seems to be adhered to the surface. The transition

point is qualitatively reminiscent of the onset of the irreversible elastohydrodynamic adhesion regime described in this section.

A ball-park example of the applicability of these results may be the estimation of the lift-off shear rate for a spherical particle near a deformable and sticky substrate, as sketched in figure 13(*e*). Earlier works (Goldman, Cox & Brenner 1967*a*; O'Neill 1968) have shown that the viscous drag force and torque on a neutrally buoyant sphere, in a slow linear shear flow near a rigid wall, are $F_x = 1.7005 \times 6\pi\mu\gamma a^2$ and $T_y = 0.4719 \times 8\pi\mu\gamma a^3$, where γ is the undisturbed shear rate. Equating these two results to the leading-order force and torque (4.6) and (4.10), and neglecting $O(\eta_0\Upsilon, \eta_0\Xi)$ terms in the drag force, the non-dimensional rotational velocity of the sphere induced by the shear flow becomes $\omega = 0.567$ to maintain dynamical equilibrium, with $\beta = \pi/2$. The lift-off shear rate is found to be

$$\gamma_L \approx \left[\frac{2.403 + \ln(a/\delta)}{2.451}\right] \sqrt{\frac{(A_{sfw} - 768 c_i N_A k T \lambda \ell_D \delta^2 \pi \mathrm{e}^{-\delta/\ell_D}) E (1-\nu)\delta}{\pi\mu^2 \ell a^3 (1+\nu)(1-2\nu)}}, \tag{6.3}$$

which increases with the substrate stiffness and intermolecular attraction. The shear rate can be increased up to the critical shear rate for irreversible elastohydrodynamic adhesion, for which $\eta_{0L} = \eta_{0C}$, which value depends on the particular relative intensity of the intermolecular parameters.

If the DLVO criterion (2.22) is used, the critical ionic concentration $c_i^\triangledown$ for adhesion can be obtained by solving the system of equations

$$\left.\begin{aligned}
&1 - \left(\frac{c_{i0}^\triangledown}{c_i^\triangledown}\right)^{1/2} (\kappa^\triangledown)^2 \mathrm{e}^{-(\kappa^\triangledown - 1)} + \eta_{0\triangledown}\left\{\Upsilon_\triangledown\left[\frac{1}{(\kappa^\triangledown)^4}\left(\frac{c_i^\triangledown}{c_{i0}^\triangledown}\right)^2 + \left(\frac{c_i^\triangledown}{4c_{i0}^\triangledown}\right)(\kappa^\triangledown)^2 \mathrm{e}^{-2(\kappa^\triangledown - 1)}\right.\right. \\
&\quad \left.\left. - \left(\frac{c_i^\triangledown}{c_{i0}^\triangledown}\right)^{3/2} \frac{\mathrm{e}^{-(\kappa^\triangledown - 1)}}{\kappa^\triangledown}\right] - \frac{48}{125\Upsilon_\triangledown \kappa^\triangledown}\left(\frac{c_i^\triangledown}{c_{i0}^\triangledown}\right)^{1/2}\right\} = O(\eta_{0\triangledown}^2), \\
&1 - \left(\frac{c_{i0}^\triangledown}{c_i^\triangledown}\right)^{1/2} \kappa^\triangledown \mathrm{e}^{-(\kappa^\triangledown - 1)} + \eta_{0\triangledown}\left\{\Upsilon_\triangledown\left[\frac{1}{5(\kappa^\triangledown)^4}\left(\frac{c_i^\triangledown}{c_{i0}^\triangledown}\right)^2 + \left(\frac{c_i^\triangledown}{8c_{i0}^\triangledown}\right)(\kappa^\triangledown) \mathrm{e}^{-2(\kappa^\triangledown - 1)}\right.\right. \\
&\quad \left.\left. - \left(\frac{c_i^\triangledown}{c_{i0}^\triangledown}\right)^{3/2} \frac{\mathrm{e}^{-(\kappa^\triangledown - 1)}}{\kappa^\triangledown} m(\kappa)\right] - \frac{24}{125\Upsilon_\triangledown \kappa^\triangledown}\left(\frac{c_i^\triangledown}{c_{i0}^\triangledown}\right)^{1/2}\right\} = O(\eta_{0\triangledown}^2),
\end{aligned}\right\} \tag{6.4}$$

where we use (5.14). In this formulation, $\eta_{0\triangledown}$ and $\Upsilon_\triangledown$ are based on $\delta_{0\triangledown}$, and $m(\kappa)$ is given by (B 4). It can be shown that the expansions

$$\frac{c_i^\triangledown}{c_{i0}^\triangledown} = 1 - \eta_{0\triangledown}\left(0.053\Upsilon_\triangledown - \frac{48}{125\Upsilon_\triangledown}\right) + \cdots \tag{6.5}$$

$$\kappa^\triangledown = 1 + \eta_{0\triangledown}\left(0.223\Upsilon_\triangledown - \frac{24}{125\Upsilon_\triangledown}\right) + \cdots \tag{6.6}$$

are asymptotic solutions of (6.4) for $\eta_{0\triangledown} \ll 1$. In particular, (6.5) represents the elastohydrodynamic correction to the critical coagulation concentration, and it shows (i) that the perturbation of the critical concentration is kinematically irreversible in which it does not depend on the velocity direction, and (ii) that the critical concentration decreases with increasing $\eta_{0\triangledown}$ if the van der Waals force is strong enough to outweigh the elastohydrodynamic repulsion, $\Upsilon_\triangledown > 2.691$, and increases with increasing $\eta_{0\triangledown}$ if the van der Waals force is small enough such that the repulsive elastohydrodynamic effect prevails, $\Upsilon_\triangledown < 2.691$. The elastostatic result (B 5) recovered

in the limit of small non-dimensional velocities $\Upsilon_\nabla \gg 2.691$. Therefore, sufficiently large non-dimensional velocities $\Upsilon_\nabla < 2.691$ contribute to suppress adhesion by electrolyte addition. Note that $\Upsilon = (\delta_0^\nabla/\delta)^{3/2}\Upsilon_\nabla < \Upsilon_\nabla$ and $\eta_0 = (\delta_0^\nabla/\delta)^{5/2}\eta_{0\nabla} < \eta_{0\nabla}$, so that the expansion (6.5) is valid for quite small values of η_0 since $\eta_0 < \eta_{0\nabla} \ll 1$, for which the elastohydrodynamic barrier is small, thereby enhancing adhesion for sufficiently reduced electric repulsion. Equation (6.5) models adhesion in the hypothetical case that elastic instabilities are negligible in the range $\delta_0^\nabla < \delta \ll a$, which represents a good approximation for $\eta_0 < \eta_{0\nabla} \ll 1$, and if $\eta_{0\nabla}\Upsilon_\nabla < \Delta_{0C\nabla}^{vdW}$. In this formulation, $\Delta_{0C\nabla}^{vdW}$ represents the critical van der Waals compliance for irreversible elastohydrodynamic adhesion evaluated at $\eta_{0\nabla}$, $\Delta_{0\nabla}^{el}$ and κ^∇, which, to leading order in $\eta_{0\nabla}$, is given by $\Delta_{0C\nabla}^{vdW} = 0.451$ as detailed in Appendix B. If these conditions are not satisfied, the particle undergoes irreversible elastohydrodynamic adhesion before surpassing the energy barrier, and the corrected DLVO criterion (6.5) loses accuracy to describe adhesion. Similarly, if the solvent is deionized, (6.5) cannot describe adhesion.

7. General influences of the substrate thickness and material incompressibility

If the substrate material is incompressible, $\nu = 1/2$, all the results presented in the previous sections, such as the lift force, drag and drift-force perturbations, lift-off and hydrodynamic adhesion compliances, lift-off shear rate and corrections to the critical concentration, become zero; the substrate behaves as a rigid wall to leading order in the non-dimensional layer thickness ζ, as noticed in Appendix A. To obtain the influences of the incompressibility effects, higher-order terms in the ζ asymptotic expansion of the surface deformation must be retained. If (A 20) is used, it can be shown that a substrate composed of a thin layer of incompressible material develops the same type of elastic instability for sufficiently large van der Waals compliances as the one presented in Appendix B, and that, in the absence of electric forces, the critical van der Waals compliance for elastostatic adhesion is $\Delta_{2C}^{vdW} = 0.013$. Using (A 20) and following the same procedures as in § 5, the lift force on a gliding particle near an incompressible substrate

$$F_z = \frac{\pi\mu U \mathscr{V}(\omega,\beta)a}{\epsilon^{1/2}}\left\{-\Upsilon + \frac{2\Xi}{\kappa} + \eta_2\left[\frac{1296}{875} - \kappa\Xi^2 - \frac{18\Upsilon^2}{7} + \Upsilon\Xi\kappa\left[2\kappa^3 e^\kappa \mathrm{Ei}(-\kappa) + 2\kappa^2 - 2\kappa + 4\right]\right] + \cdots\right\} \tag{7.1}$$

is obtained, where η_2 is given by (A 18). Similar to the lift force (5.14) for the case of a compressible layer, the sum of the mixed terms of $O(\eta_2\Upsilon^2, \eta_2\Xi^2, \eta_2\Upsilon\Xi)$ in (7.1) always has a negative sign independent of the values of Υ and Ξ, which induces a non-additivity in the intermolecular forces, and it represents the perturbation of the intermolecular force on a stationary sphere near an incompressible deformable substrate. The lift-off hydrodynamic compliance is given by

$$\eta_{2L} \approx \left\{\frac{125}{48}\left[\Delta_2^{vdW} - \frac{2\Delta_2^{el}}{\kappa} + \kappa\Delta_2^{el^2} + \frac{18}{7}\Delta_2^{vdW^2} - \Delta_2^{vdW}\Delta_2^{el}\kappa\left[2\kappa^3 e^\kappa \mathrm{Ei}(-\kappa) + 2\kappa^2 - 2\kappa + 4\right]\right]\right\}^{1/2}, \tag{7.2}$$

where Δ_2^{vdW} and Δ_2^{el} are given by (A 25) and (A 26) respectively. Since $\eta_2^{vdW}/\eta_0 = O(\zeta^2) \ll 1$, $\Delta_2^{vdW}/\Delta_0^{vdW} = O(\zeta^2) \ll 1$ and $\Delta_{el}^{vdW}/\Delta_0^{el} = O(\zeta^2) \ll 1$, the compliance of an incompressible layer under a stress load of intermolecular or hydrodynamic

origin is much less than that of a compressible layer under the same load, because of confinement effects produced by the rigid substrate, so that the material incompressibility tends to suppress the elastohydrodynamic adhesion of the particle to the substrate and reduce the elastohydromolecular effects on the forces.

In this investigation, expressions have not been derived for the lift force and lift-off compliances for the case of a semi-infinite elastic substrate. Nonetheless, the perturbation of the lift force on a particle gliding over a semi-infinite elastic medium can be assumed to scale with η_∞, which is given by (A 22), such that the hydrodynamic lift-off compliance becomes

$$\eta_{\infty L} \approx \left\{ C_3 \left[\Delta_\infty^{vdW} - \frac{2\Delta_\infty^{el}}{\kappa} + O\left(\Delta_\infty^{vdW^2}, \Delta_\infty^{el^2}\right) \right] \right\}^{1/2}, \tag{7.3}$$

where Δ_∞^{vdW} and Δ_∞^{el} are given by (A 27) and (A 28) respectively, and C_3 is an order-unity constant. The correction term of $O(\Delta_\infty^{vdW^2}, \Delta_\infty^{el^2})$ represents the perturbation of the intermolecular force on a stationary sphere near a semi-infinite elastic substrate. Since $\eta_\infty/\eta_0 = O(1/\zeta) \gg 1$, $\Delta_\infty^{vdW}/\Delta_0^{vdW} = O(1/\zeta) \gg 1$ and $\Delta_\infty^{el}/\Delta_0^{el} = O(1/\zeta) \gg 1$, the compliance of a semi-infinite elastic layer under a stress load, of intermolecular or hydrodynamic origin, is much larger than that of a thin compressible layer under the same load, so that the layer thickness tends to enhance the elastohydrodynamic adhesion of the particle to the substrate and increase the elastohydromolecular effects on the forces.

8. Conclusions

Substrate compliance and intermolecular effects on the slow translational and rotational motions of a small solid spherical particle were analytically and numerically investigated in this study by making use of a hydrodynamic lubrication approximation. Electric double-layer and van der Waals stresses were formulated to model the intermolecular influences in the gap region by using the Derjaguin approximation. The hydrodynamic compliance η and intermolecular compliances Δ^{vdW} and Δ^{el} were found to be the relevant non-dimensional parameters that characterize the relative intensity of the hydrodynamic and intermolecular stresses with respect to the restoring elastic stresses on the surface. Influences of a general particle drift motion were analysed by introducing in the formulation the rotational to translational velocity ratio ω, and the azimuth angle of orientation of the rotation axis β relative to the translation axis. A characteristic velocity $U\sqrt{1+\omega^2+2\omega\sin\beta}$ was defined as the gliding velocity for the general case of drift motion, where U is the translational velocity without drift. The formulation was applied to a substrate composed of a thin compressible elastic layer coating a rigid foundation, and special emphasis was made on the influences of attracting van der Waals forces and repulsive electric forces. Asymptotic formulas were derived in the NRWA, $\eta \ll 1$, and they were compared to numerical computations for fully deformable substrates, for which $\eta \leqslant O(1)$.

The combination of elastohydromolecular effects was found to induce irreversible and reversible elastohydrodynamic regimes, a lift force, and drag-force and drift-force disturbances, all of which appear to be new. For $\eta = \eta_L$ a reversible elastohydrodynamic regime is found. For $\eta < \eta_L$, an irreversible elastohydrodynamic regime occurs with negative lift forces. For $\eta > \eta_L$, an irreversible elastohydrodynamic regime occurs with positive lift forces. The limiting values of elastohydrodynamic adhesion and expressions of the forces were derived in the NRWA limit and compared to numerical solutions.

The lift force, which scales with even powers of the gliding velocity, is negative for large and attracting van der Waals forces, and is positive for repulsive van der Waals forces or for intermediate attracting van der Waals forces and sufficiently soft substrates. Electric intermolecular repulsion increases the magnitude of the lift force. For the same translational velocity, particle dimensions and substrate mechanical properties, the purely rolling motion ($\omega = 1$, $\beta = \pi/2$) produces a larger lift force than the corkscrew ($\omega = 1$, $\beta = 0$) and translational ($\omega = 0$) motions. In addition to the leading-order intermolecular forces, to second order in the substrate compliance, the lift force is composed of elastohydrodynamic and elastomolecular terms, the latter corresponding to the perturbation of the intermolecular force on a stationary sphere, which is always attractive and represents a non-additivity of intermolecular effects. The drag-force perturbation scales with odd powers of the velocity. Substrate compliance favours a drag-force reduction. The coupling between intermolecular and elasticity effects induces a van der Waals drag force and an electric drag force. In general, intermolecular attractive forces increase the drag on the sphere, and the contrary holds for repulsive forces. For the same translational velocity, particle dimensions and substrate mechanical properties, the pure rolling motion ($\omega = 1$, $\beta = \pi/2$) produces a larger drag-force reduction than the corkscrew ($\omega = 1$, $\beta = 0$) and translational ($\omega = 0$) motions. Substrate-deformation effects are found to play a very weak role on the drift force. Attractive intermolecular forces produce small increments on the drift force because of a viscous-traction enhancement, and the contrary holds for repulsive forces.

A reversible elastohydrodynamic adhesion regime was found in both ionized and deionized solvents for a lift-off hydrodynamic compliance $\eta = \eta_L$, the value of which increases with Δ^{vdW} and decreases with increasing Δ^{el}. In this regime, particle lateral motion and lift-off from the wall can occur. The lift-off hydrodynamic compliance can be achieved by sufficiently large gliding velocities or substrate compliances. This regime ceases to exist if the gliding motion stops, and it is found to be stable against small gap disturbances at constant gliding power.

In the region $\eta < \eta_L$, the particle is subject to a negative lift, and an irreversible elastohydrodynamic adhesion regime occurs for sufficiently large Δ^{vdW}. This irreversible adhesion mechanism is found in both ionized and deionized solvents, and is induced by elastic instabilities in the form of surface bifurcations in the substrate, which have been studied in Appendix B in its elastostatic version for a stationary sphere near a deformable substrate. The limiting values for irreversible elastohydrodynamic adhesion are given by the critical hydrodynamic compliance $\eta = \eta_C$, which were numerically calculated. The compliance η_C was found to increase with Δ^{vdW} and decrease with increasing Δ^{el}.

In the region $\eta > \eta_L$, the particle is subject to a positive lift force, but an irreversible elastohydrodynamic adhesion regime can take place because the substrate becomes softer and more unstable as η_0 increases. In this regime, adhesion is enhanced by sufficiently large substrate compliances and gliding velocities.

An increase in the repulsive electric force tends to suppress elastohydrodynamic adhesion. However, elastohydrodynamic adhesion can occur and be suppressed in deionized solvents, where there is no electrical repulsion, and cannot be described by the classic DLVO theory of colloid stabilization.

Elastohydrodynamic corrections to the DLVO critical coagulation concentration, for which the energy barrier against Brownian perturbations of the gap distance is small, were obtained in the NRWA limit for very small η, such that the elastohydrodynamic barrier was also small, which showed that the critical

concentration decreases with increasing η because of an enhancement of the attractive van der Waals force; this trend continues up to a critical van der Waals to hydrodynamic stress ratio η/Δ^{vdW}, above which the elastohydrodynamic repulsion dominates and the critical coagulation concentration increases with η. The corrected DLVO critical concentration may be accurate to describe the adhesion process for sufficiently small compliances such that the elastic substrate remains in static mechanical equilibrium, but loses accuracy for low-midway compliances for which elastohydrodynamic adhesion occurs before the particle has surpassed the energy barrier, and it is not applicable when the solvent is deionized.

Material incompressibility in the substrate is found to suppress adhesion, and formulas for the lift force and lift-off hydrodynamic compliance have been derived for a fully incompressible substrate. A semi-infinite elastic substrate is shown to enhance adhesion and elastohydromolecular effects by having larger hydrodynamic and intermolecular compliances, which may represent an important feature to account for in future numerical work and laboratory experiments.

The results obtained in this study show that the mechanical and surface properties of the substrate and the gliding kinematic characteristics of the particle have important influences on the adhesive and migrating behaviours, and therefore potential benefits in practical applications, such as particle and cell manipulations in microfluidics systems, may be obtained by modifying those magnitudes to enhance or suppress dynamical phenomena like lift-off from the surface and drag reduction.

The author is indebted to Professor F. A. Williams, Professor J. C. Lasheras and Professor A. L. Sánchez for their extraordinary mentorship. The author is also grateful to Professor S. H. Davis, Professor E. Lauga and Professor J. C. Del Álamo for thoughtful suggestions on earlier drafts and to Dr. B. Alonso-Latorre and Dr. G. Mauger for encouraging this investigation.

Appendix A. Substrate mechanics

In this analysis, the substrate is modelled by a compliant layer of thickness ℓ coating a rigid foundation as depicted in figure 1. The material of the layer is assumed to be isotropic and characterized by its Young modulus E and Poisson coefficient ν, with $0<\nu<1/2$ for highly compressible materials such as gels, and $\nu\sim 1/2$ for highly incompressible materials such as elastomers, for which the Poisson effect becomes primarily important. The solid stress tensor $\boldsymbol{\sigma}$ satisfies the internal equilibrium equation

$$\boldsymbol{\nabla}\cdot\boldsymbol{\sigma}=0 \tag{A 1}$$

in the absence of volumetric forces in the thin layer and is related to the displacement vector $\boldsymbol{u}$ by the linear constitutive equation

$$\boldsymbol{\sigma}=\frac{E(\boldsymbol{\nabla u}+\boldsymbol{\nabla u}^{\mathrm{T}})}{2(1+\nu)}+\frac{\nu E(\boldsymbol{\nabla}\cdot\boldsymbol{u})\boldsymbol{I}}{(1+\nu)(1-2\nu)}, \tag{A 2}$$

subject to boundary conditions of solid–liquid interface equilibrium and compatibility of deformations with the rigid foundation

$$\boldsymbol{\sigma}\cdot\boldsymbol{n}^{\mathrm{T}}=\boldsymbol{\sigma}^{\bigstar}\cdot\boldsymbol{n}^{\mathrm{T}}\quad\text{at}\quad z=-H,\quad\text{and}\quad\boldsymbol{u}=0\quad\text{at}\quad z=-\ell, \tag{A 3}$$

where $\boldsymbol{\sigma}^{\bigstar}=-P^{\bigstar}\boldsymbol{I}+\mu(\boldsymbol{\nabla v}+\boldsymbol{\nabla v}^{\mathrm{T}})$ is the hydromolecular stress tensor, which is composed of the sum of the isotropic hydromolecular pressure tensor and the deviatoric viscous stress tensor. In this formulation, $\boldsymbol{n}=(-\partial u_z/\partial r|_{z=0},-r^{-1}\partial u_z/$

$\partial\varphi|_{z=0}, 1) + O(\epsilon)$ is a unit vector normal to the substrate surface. Equations (A 1)–(A 3) are generally coupled to the lubrication problem (2.11) and (2.12) in a rather cumbersome way for arbitrary layer thickness ℓ. An asymptotic analysis of this complicated problem can be performed by assuming that the ratio of the layer thickness ℓ to the characteristic lubrication region dimension $\delta/\epsilon^{1/2}$ is a small parameter:

$$\zeta = \frac{\epsilon^{1/2}\ell}{\delta} \ll 1, \tag{A 4}$$

so that the layer thickness ℓ may well be much larger than the minimum gap distance δ since $\ell/\delta \ll 1/\epsilon^{1/2}$ and $\epsilon \ll 1$, but sufficiently small compared with the particle radius, $\ell/a \ll \epsilon^{1/2}$. This appendix obtains the surface deformation, by solving asymptotically (A 1)–(A 3), as a function of $P^{\star}$ and the hydrodynamic compliance η, for $\eta = O(1)$ and $\zeta \ll 1$.

The qualitative asymptotic behaviour of the solution can be readily extracted from an order of magnitude analysis of (A 1)–(A 3). Surface loads of order unity applied on the thin layer are expected to produce a compression normal stress $\sigma_{zz} = O(1)$ and a vertical deformation $u_z = O(\zeta)$. The Poisson effect produces radial and azimuthal normal stresses $\sigma_{rr} = O(1)$ and $\sigma_{\varphi\varphi} = O(1)$ and displacements $u_r = O(\zeta^2)$ and $u_\varphi = O(\zeta^2)$. For nearly incompressible materials, $\nu \sim 1/2$, the stresses become independent of the material properties in the first approximation, and the vertical displacement becomes $u_z = O(\zeta^3)$ to satisfy the vanishing cubical dilatation constraint $\nabla \cdot \boldsymbol{u} = 0$ in the incompressible limit (Landau & Lifshitz 1959).

Equations (A 1)–(A 3) are non-dimensionalized with ℓ as the unit of vertical coordinate, $\delta/\epsilon^{1/2}$ as the unit of radial coordinate, δ as the unit of vector displacement and $E(1-\nu)\delta/[\ell(1+\nu)(1-2\nu)]$ as the unit of stress tensor. In these variables, (A 1) and (A 2) become

$$\left.\begin{aligned} \frac{\partial\sigma_{rz}}{\partial z} + \zeta\left[\frac{1}{r}\frac{\partial}{\partial r}(r\sigma_{rr}) + \frac{1}{r}\frac{\partial\sigma_{r\varphi}}{\partial\varphi} - \frac{\sigma_{\varphi\varphi}}{r}\right] &= 0, \\ \frac{\partial\sigma_{\varphi z}}{\partial z} + \zeta\left[\frac{1}{r}\frac{\partial}{\partial r}(r\sigma_{r\varphi}) + \frac{1}{r}\frac{\partial\sigma_{\varphi\varphi}}{\partial\varphi} + \frac{\sigma_{r\varphi}}{r}\right] &= 0, \\ \frac{\partial\sigma_{zz}}{\partial z} + \zeta\left[\frac{1}{r}\frac{\partial}{\partial r}(r\sigma_{rz}) + \frac{1}{r}\frac{\partial\sigma_{z\varphi}}{\partial\varphi}\right] &= 0, \end{aligned}\right\} \tag{A 5}$$

and

$$\left.\begin{aligned} \sigma_{rr} &= \frac{\nu}{1-\nu}\frac{\partial u_r}{\partial z} + \left[\frac{\partial u_r}{\partial r} + \frac{\nu}{1-\nu}\left(\frac{u_r}{r} + \frac{1}{r}\frac{\partial u_\varphi}{\partial\varphi}\right)\right]\zeta, \\ \sigma_{r\varphi} &= \frac{1-2\nu}{2(1-\nu)}\left[r\frac{\partial}{\partial r}\left(\frac{u_\varphi}{r}\right) + \frac{1}{r}\frac{\partial u_r}{\partial\varphi}\right]\zeta, \\ \sigma_{rz} &= \frac{1-2\nu}{2(1-\nu)}\left(\frac{\partial u_r}{\partial z} + \zeta\frac{\partial u_z}{\partial r}\right), \\ \sigma_{\varphi\varphi} &= \frac{1-2\nu}{1-\nu}\left(\frac{1}{r}\frac{\partial u_\varphi}{\partial\varphi} + \frac{u_r}{r}\right)\zeta + \frac{\nu}{1-\nu}\left[\frac{\partial u_z}{\partial z} + \zeta\left(\frac{1}{r}\frac{\partial}{\partial r}(ru_r) + \frac{1}{r}\frac{\partial u_\varphi}{\partial\varphi}\right)\right], \\ \sigma_{\varphi z} &= \frac{1-2\nu}{2(1-\nu)}\left(\frac{\partial u_\varphi}{\partial z} + \frac{\zeta}{r}\frac{\partial u_z}{\partial\varphi}\right), \\ \sigma_{zz} &= \frac{\partial u_z}{\partial z} + \frac{\nu}{1-\nu}\left[\frac{1}{r}\frac{\partial}{\partial r}(ru_r) + \frac{1}{r}\frac{\partial u_\varphi}{\partial\varphi}\right]\zeta. \end{aligned}\right\} \tag{A 6}$$

The regular asymptotic expansions

$$\left.\begin{aligned}\boldsymbol{\sigma} &= \boldsymbol{\sigma_0} + \zeta\boldsymbol{\sigma_1} + \zeta^2\boldsymbol{\sigma_2} + O(\zeta^3)\\ \boldsymbol{u} &= \boldsymbol{u_0} + \zeta\boldsymbol{u_1} + \zeta^2\boldsymbol{u_2} + O(\zeta^3),\end{aligned}\right\} \tag{A 7}$$

are substituted into (A 5) and (A 6). The hydrodynamic compliance η defined in § 2 is described below by an asymptotic expansion of the form

$$\eta = \hat{\eta}_0 + \zeta^2\hat{\eta}_2 + O(\zeta^4), \tag{A 8}$$

where $\hat{\eta}_i = \eta_i/\zeta^i$. To leading order in ζ, (A 5) and (A 6) reduce to

$$\frac{\partial^2 u_{r0}}{\partial z^2} = \frac{\partial^2 u_{\varphi 0}}{\partial z^2} = \frac{\partial^2 u_{z0}}{\partial z^2} = 0, \tag{A 9}$$

subject to $u_{r0} = u_{\varphi 0} = u_{z0} = 0$ on $z = -1$ and $\partial u_{z0}/\partial z = -\eta_0 P^\bigstar$ at $z = 0$. In this formulation, the hydrodynamic compliance η_0 is given by

$$\eta_0 = \frac{\mu U \mathscr{V}(\omega, \beta)\ell a^{1/2}(1+\nu)(1-2\nu)}{E(1-\nu)\delta^{5/2}}. \tag{A 10}$$

The leading-order stresses and deformations are given by

$$\sigma_{rr0} = \sigma_{\varphi\varphi 0} = -\frac{\nu\eta_0 P^\bigstar}{1-\nu}, \quad \sigma_{zz0} = -\eta_0 P^\bigstar, \quad \sigma_{r\varphi 0} = \sigma_{rz0} = \sigma_{\varphi z0} = 0,$$

and

$$u_{r0} = u_{\varphi 0} = 0, \quad u_{z0} = -\eta_0 P^\bigstar (1+z), \tag{A 11}$$

which resemble the classic rigid foundation model (Johnson 1985), in which the wall deflection is proportional to the net normal stress (intermolecular and hydrodynamic stresses). If the Poisson effect is negligible, the leading-order radial and azimuthal normal stresses vanish in the first approximation because of the large material compressibility. If the Poisson effect is important, $\nu \sim 1/2$, the hydrodynamic compliance η_0 and elastic displacements vanish in this approximation, giving no useful information of the deformation field, for which higher-order terms must be retained. It is worth mentioning that, for large hydrodynamic compliances, $\eta_0 = O(\epsilon^{-1/2}) \gg 1$, the boundary condition $\partial u_{z0}/\partial z = -\eta_0 P^\bigstar$ at $z = 0$ becomes inaccurate in this approximation, because the curvature of the surface may produce non-negligible viscous shear forces, thereby producing non-negligible contributions by the non-diagonal terms of the hydromolecular stress tensor to the surface deformation field.

To second order in ζ, (A 5) and (A 6) become

$$\frac{\partial^2 u_{r1}}{\partial z^2} = \frac{\eta_0}{1-2\nu}\frac{\partial P^\bigstar}{\partial r}, \quad \frac{\partial^2 u_{\varphi 1}}{\partial z^2} = \left(\frac{\eta_0}{1-2\nu}\right)\frac{1}{r}\frac{\partial P^\bigstar}{\partial \varphi}, \quad \frac{\partial^2 u_{z1}}{\partial z^2} = 0, \tag{A 12}$$

subject to $u_{r1} = u_{\varphi 1} = u_{z1} = 0$ at $z = -1$ and $\partial u_{r1}/\partial z = \partial u_{\varphi 1}/\partial z = \partial u_{z1}/\partial z = 0$ at $z = 0$, solutions to which yield the second-order stresses and deformations

$$\sigma_{rr1} = \sigma_{\varphi\varphi 1} = \sigma_{zz1} = \sigma_{r\varphi 1} = 0, \quad \sigma_{r\varphi 1} = \left(\frac{\nu\eta_0 z}{1-\nu}\right)\frac{\partial P^\bigstar}{\partial r}, \quad \sigma_{\varphi z1} = \left(\frac{\nu\eta_0 z}{1-\nu}\right)\frac{1}{r}\frac{\partial P^\bigstar}{\partial \varphi},$$

and

$$u_{r1} = \frac{\eta_0(z^2-1)}{2(1-2\nu)}\frac{\partial P^\star}{\partial r}, \quad u_{\varphi 1} = \frac{\eta_0(z^2-1)}{2(1-2\nu)}\frac{1}{r}\frac{\partial P^\star}{\partial \varphi}, \quad u_{z1} = 0, \tag{A 13}$$

so that the second-order correction to the vertical displacement is zero.

Finally, to third order in ζ, (A 5) and (A 6) become

$$\frac{\partial^2 u_{r2}}{\partial z^2} = \frac{\partial^2 u_{\varphi 2}}{\partial z^2} = 0, \quad \frac{\partial^2 u_{z2}}{\partial z^2} = -\frac{2\nu\eta_0 z}{1-2\nu}\nabla_\perp^2 P^\star, \tag{A 14}$$

subject to $u_{r2} = u_{\varphi 2} = u_{z2} = 0$ at $z = -1$, and

$$\frac{\partial u_{r2}}{\partial z} = \frac{\partial u_{\varphi 2}}{\partial z} = 0, \quad \frac{\partial u_{z2}}{\partial z} = \frac{\nu\eta_0\nabla_\perp^2 P^\star}{2(1-\nu)(1-2\nu)}, \tag{A 15}$$

at $z = 0$, solutions to which give the displacement field

$$\left.\begin{aligned} u_{r2} &= u_{\varphi 2} = 0, \\ u_{z2} &= \frac{\nu\eta_0\nabla_\perp^2 P^\star}{1-2\nu}\left[-\frac{z^3}{3} + \frac{z}{2(1-\nu)} + \frac{1+2\nu}{6(1-\nu)}\right]. \end{aligned}\right\} \tag{A 16}$$

The asymptotic deformation field given by (A 11), (A 13) and (A 16) yields zero cubical dilatation $\nabla\cdot\boldsymbol{u} = 0$ to $O(\zeta^3)$ in the incompressible limit $\nu \sim 1/2$.

According to (A 11), (A 13) and (A 16), the substrate deflection

$$u_z = -\eta_0 P^\star + \eta_2\nabla_\perp^2 P^\star + O(\zeta^3) \quad \text{at} \quad z = 0 \tag{A 17}$$

is found, with the higher-order hydrodynamic compliance η_2 given by

$$\eta_2 = \frac{\mu U \curlyvee(\omega, \beta)\ell^3}{E a^{1/2}\delta^{7/2}}. \tag{A 18}$$

Note that neither η_2 nor u_{z3} vanish in the incompressible limit $\nu \sim 1/2$.

For compressible materials, the rigid foundation model

$$H = P^\star = P - \frac{\curlyvee}{[h_0(r) + \eta_0 H]^3} + \Xi \mathrm{e}^{-\kappa[h_0(r)+\eta_0 H - 1]} \tag{A 19}$$

represents the first approximation of the substrate deformation, with the hydrodynamic compliance appearing implicitly in the Reynolds equation (2.11) given by (A 10). For incompressible materials $\nu \sim 1/2$, the vertical displacement becomes $O(\zeta^3)$ and (A 17) yields

$$H = -\nabla_\perp^2 P^\star = -\nabla_\perp^2 P + \nabla_\perp^2\left\{\frac{\curlyvee}{[h_0(r) + \eta_2 H]^3} - \Xi \mathrm{e}^{-\kappa[h_0(r)+\eta_2 H - 1]}\right\} \tag{A 20}$$

as an approximation valid to $O(\zeta^3)$, with η_2 given by (A 18). Expression (A 20) represents a much simpler approximation than usual solutions of the deformation field of incompressible layers based on Hankel transforms (Landau & Lifshitz 1959; Johnson 1985) and allows the acquisition of asymptotic solutions to the lubrication problem (2.11) and (2.12) for $\eta_2 \ll 1$.

In the asymptotic limit of very thick elastic substrates $\zeta \to \infty$, the surface displacement can be obtained by the method of Green's functions as detailed in classic texts of elasticity theory (Landau & Lifshitz 1959; Johnson 1985). In the

present notation, the surface deformation becomes

$$H = \int_0^{2\pi} \int_0^{\infty} \frac{P^{\bigstar}(r', \varphi') r' \, \mathrm{d}r' \, \mathrm{d}\varphi'}{\sqrt{r'^2 + r^2 - 2rr' \cos(\varphi - \varphi')}}, \tag{A 21}$$

with

$$\eta_\infty = \frac{\mu U \curlyvee(\omega, \beta) a(1 - \nu^2)}{\pi E \delta^2}, \tag{A 22}$$

the hydrodynamic compliance for semi-infinite (compressible or incompressible) elastic substrates.

Quantities similar to those represented by the hydrodynamic compliances (A 10), (A 18) and (A 22) can be obtained to describe the substrate compliance due to the action of the intermolecular stresses. The van der Waals and electric compliances are defined as

$$\Delta_0^{vdW} = \eta_0 \Upsilon = \frac{A_{sfw} \ell (1 + \nu)(1 - 2\nu)}{6\pi E (1 - \nu) \delta^4} \tag{A 23}$$

and

$$\Delta_0^{el} = \eta_0 \Xi = \frac{64(1 + \nu)(1 - 2\nu) \ell c_i N_A k T}{E(1 - \nu)\delta} \lambda\big(\Psi_w^d, \Psi_s^d\big) \mathrm{e}^{-\kappa} \tag{A 24}$$

for thin compressible elastic layers,

$$\Delta_2^{vdW} = \eta_2 \Upsilon = \frac{A_{sfw} \ell^3}{6\pi a E \delta^5} \tag{A 25}$$

and

$$\Delta_2^{el} = \eta_2 \Xi = \frac{64 \ell^3 c_i N_A k T}{E a \delta^2} \lambda\big(\Psi_w^d, \Psi_s^d\big) \mathrm{e}^{-\kappa} \tag{A 26}$$

for thin incompressible elastic layers, and

$$\Delta_\infty^{vdW} = \eta_\infty \Upsilon = \frac{A_{sfw} a^{1/2} (1 - \nu^2)}{6\pi^2 E \delta^{7/2}} \tag{A 27}$$

and

$$\Delta_\infty^{el} = \eta_\infty \Xi = \frac{64(1 - \nu^2) a^{1/2} c_i N_A k T}{\pi E \delta^{1/2}} \lambda\big(\Psi_w^d, \Psi_s^d\big) \mathrm{e}^{-\kappa}, \tag{A 28}$$

for semi-infinite elastic substrates.

The lubrication problem (2.11) and (2.12) is closed by either (A 19), (A 20) or (A 21). The semi-infinite elastic substrate equation (A 21) yields a three-dimensional nonlinear partial integro-differential equation when coupled with the lubrication problem (2.11) and (2.12) that represents quite an analytical challenge, because the hydromolecular pressure is generally a two-dimensional field. In this analysis, emphasis is mainly made on the more analytically tractable thin-layer configurations (A 19) and (A 20), because a thorough physical understanding of these cases, which could be extended to more involved situations, can be achieved by deriving exact solutions and using asymptotic methods. Section 7 briefly addresses the influences of material incompressibility and layer thickness.

Appendix B. Elastostatic adhesion and surface bifurcations in the substrate

In this appendix, the much simpler problem of a stationary sphere standing off at some distance δ from the wall surface, which represents an effective zero-Reynolds-number regime, is analysed and used to exemplify the interaction of

substrate-deformation effects with the intermolecular forces. Since there is no particle motion, $U=0$ and $\Omega=0$, the hydrodynamic pressure is zero in the gap region (i.e. the difference between the ambient pressure and the absolute hydrodynamic pressure in the gap is zero). The van der Waals and electric forces, (4.1) and (4.2), need to be corrected to account for the substrate elasticity.

The balance of electric and van der Waals forces upon the axisymmetric pseudo-hertzian static indentation of a sphere to an elastic infinite half-space, in the absence of fluid flow, is the subject of study of classical theories (Johnson, Kendall & Roberts 1971; Derjaguin, Muller & Toporov 1975). For simplicity, fluid-drainage viscous effects during particle capture are neglected in this section. Thorough studies on the dynamics of two colliding soft spheres can be found elsewhere (Davis, Serayssol & Hinch 1986; Serayssol & Davis 1986), where use was also made of infinite half-space formulation and numerical solutions were sought. In this section, the analysis is restrained to a simple description of the quasi-static stability of the flat elastic layer, which leads to estimates of the parametric ranges for which the problem (2.11) and (2.12), subject to (A 19), may have a static solution under no fluid flow, and the reasoning serves to interpret the physical meaning of the elastohydromolecular lift components of its asymptotic series calculated in § 5.1 for the gliding sphere.

In the absence of fluid motion, the wall constitutive equation (A 19) becomes

$$H = \Delta_0^{el} \mathrm{e}^{-\kappa[h_0(r)+H-1]} - \frac{\Delta_0^{vdW}}{[h_0(r)+H]^3}. \tag{B 1}$$

In this appendix, H represents the wall surface deformation non-dimensionalized with the minimum gap clearance δ. Equation (B 1) represents the equilibrium balance between the elastic, electric and van der Waals stresses on the substrate surface.

To unveil the influences of the substrate compliance effects, the asymptotic expansion of the surface deformation $H = H_0 + \Delta_0^{vdW} H_1 + \Delta_0^{vdW^2} H_2 + O(\Delta_0^{vdW^3})$, for $\Delta_0^{vdW} \ll 1$, is introduced in (B 1) by keeping the ratio of electric and van der Waals characteristic stresses $\Delta_0^{el}/\Delta_0^{vdW}$ as an order-unity parameter, which yields the elastomolecular force

$$\begin{aligned} F_z = &-\Delta_0^{vdW} + \frac{2\Delta_0^{el}}{\kappa} - \left(\Delta_0^{vdW} - \Delta_0^{el}\right)^2 - 3\Delta_0^{vdW^3} + \Delta_0^{vdW^2}\Delta_0^{el}(\kappa+6) \\ &- \Delta_0^{vdW^2}\Delta_0^{el^2}(2\kappa+3) + \kappa\Delta_0^{el^3} + O\left(\Delta_0^{vdW^4}, \Delta_0^{el^4}\right). \end{aligned} \tag{B 2}$$

In this formulation, F_z is non-dimensionalized with the characteristic elastic force $\pi E(1-\nu)\delta^2 a/\ell(1+\nu)(1-2\nu)$. The first two terms in (B 2) represent the well-known van der Waals and electric double-layer forces (4.1) and (4.2) on a sphere near a rigid wall. The remaining are correction terms that correspond to perturbations introduced by the substrate elasticity, which show that the electric and van der Waals components of the intermolecular force are not generally additive when acting on a deformable wall. The asymptotic expression (B 2) is compared in figure 14(*a*) with the numerical solution of (B 1) for deionized solvents. Note that according to (B 2), the first perturbation introduced by the deformable wall is to enhance the attracting effect in the case of attractive intermolecular forces ($\Delta_0^{vdW} > 0$ or $\Delta_0^{el} < 0$) due to an effective reduction in the gap size, and to suppress the effect of repulsion in the case of repulsive intermolecular forces ($\Delta_0^{vdW} < 0$ or $\Delta_0^{el} > 0$) due to an effective increase on the gap size. For $\Delta_{0L}^{vdW} \sim 2\Delta_0^{el}/\kappa$, the force on the sphere is zero in the first approximation. For $\Delta_0^{vdW} < \Delta_{0L}^{vdW}$, the force on the sphere is repulsive, and the opposite occurs for $\Delta_0^{vdW} > \Delta_{0L}^{vdW}$.

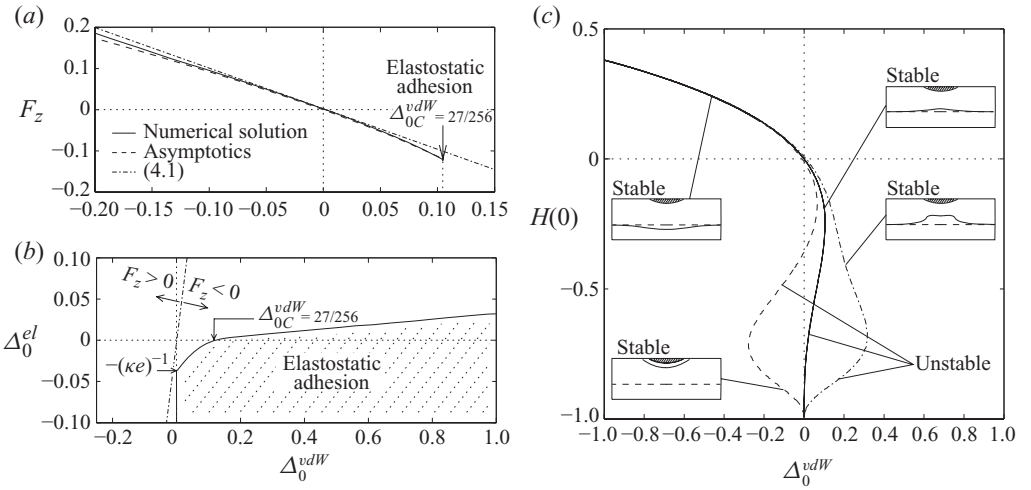

FIGURE 14. (*a*) Non-dimensional normal force on the sphere as a function of the van der Waals compliance for deionized solvents. (*b*) Map of static solutions, for a stationary sphere, in terms of the electric compliance Δ_0^{el} and the van der Waals compliance Δ_0^{vdW}; the hatched area denotes the occurrence of elastostatic adhesion or non-existence of a static solution, which represents an elastic instability produced by the unbounded attracting van der Waals or electric stresses, and is bounded by the critical compliance Δ_{0C}^{vdW} (solid line). The dot-dashed line denotes the compliance Δ_{0L}^{vdW} for $F_z = 0$. (*c*) Centerline elastic displacement of the substrate as a function of the van der Waals compliance for deionized solvents (solid line), repulsive (dot-dashed line) and attractive (dashed line) electric forces. Insets show typical radial deformation profiles in each branch. Calculations are performed here for $\kappa = 10$.

Further examination of (B 1) shows the existence of bifurcations in the solution of the displacement field. Particularizing (B 1) for attracting van der Waals forces $\Delta_0^{vdW} > 0$ and repulsive electric forces $\Delta_0^{el} > 0$, which may correspond to the most usual physical configuration (Israelachvili 1985; Poortinga *et al.* 2002; Lyklema 2005), shows that as Δ_0^{vdW} increases, the elastic deformation towards the sphere side increases, reaching a turning point at which the wall surface develops an unstable sharp cusp along the axis $r = 0$, which is representative of elastostatic adhesion or capture of the stationary particle by the elastic substrate for a minimum compliance $\Delta_{0C}^{vdW} = \Delta_{0C}^{vdW}(\Delta_0^{el}, \kappa)$, in the sense that no equilibrium solution of (B 1) exists for $\Delta_0^{vdW} > \Delta_{0C}^{vdW}$, as shown in figure 14(*c*). In this regime, the critical compliance Δ_{0C}^{vdW} increases with the electric–elastic stress ratio Δ_0^{el}, as observed in figure 14(*b*), and decreases with increasing κ, with $\Delta_{0C}^{vdW} = 27/256$ for deionized solvents $\Delta_0^{el} = 0$. For $\Delta_0^{vdW} < \Delta_{0C}^{vdW}$ with $\Delta_0^{vdW} > 0$, two equilibrium solutions of (B 1) may exist for the same value of Δ_0^{vdW}, with the low-strained solution being the stable solution. The high-strained solution is unstable, in which a small perturbation on the surface deformation towards the sphere side produces a steeper increment of the intermolecular traction stress compared with the corresponding increments undergone by the electric and internal restoring elastic stresses in the layer, so that the wall surface departs from static equilibrium and adhesion occurs with $H = -h_0(r)$. A similar description holds for the case of attractive van der Waals and electric forces, $\Delta_0^{vdW} > 0$ and $\Delta_0^{el} < 0$.

In the absence of van der Waals forces, $\Delta_0^{vdW} = 0$, elastostatic adhesion occurs for sufficiently attractive electric forces $\Delta_0^{el} < \Delta_{0C}^{el} = -1/\kappa e$. For repulsive electric and van der Waals forces, $\Delta_0^{vdW} < 0$ and $\Delta_0^{el} > 0$, the elastic layer is always stable and a single equilibrium solution is obtained. For repulsive van der Waals forces and attractive

electric forces, $\Delta_0^{vdW} < 0$ and $\Delta_0^{el} < 0$, three solutions may be obtained for the same value of Δ_0^{vdW} resembling an S-curve, with a stable low-strained branch in which repulsion dominates, an unstable middle-branch, and a stable high-strained solution in which there is a balance between attraction, repulsion and the elastic restoring force that places the flat layer at a short equilibrium distance from the sphere surface; note that complete elastostatic adhesion (i.e. mechanical disequilibrium of the substrate) is not possible in this configuration due to the strong singularity of the van der Waals repulsive stresses.

The intermolecular force asymptotic expansion (B 2) corresponds to the low-strained stable solutions of (B 1). Note that a particle free to move will not experience elastostatic adhesion for $\Delta_0^{vdW} < \Delta_{0L}^{vdW}$ because the net intermolecular force would be repulsive. For $\Delta_0^{vdW} > \Delta_{0L}^{vdW}$, the net intermolecular force on the particle is attractive, but it is not until the gap distance δ becomes sufficiently small, such that $\Delta_0^{vdW} > \Delta_{0C}^{vdW}$, in which the elastostatic adhesive mechanism sets in.

If the DLVO criterion (2.22) is used, adhesion by random perturbations of the gap distance can occur if the electrolyte concentration is sufficiently large such that the energy barrier is small as detailed in § 2.2 and shown in figure 1. The critical ionic concentration for rapid coagulation of the sphere on the deformable substrate can be obtained by combining (2.22) and (B 2), which yields the system of equations

$$\left.\begin{aligned} &1 - \left(\frac{c_{i0}^{\triangledown}}{c_i^{\triangledown}}\right)^{1/2} (\kappa^{\triangledown})^2 \mathrm{e}^{-(\kappa^{\triangledown}-1)} + \Delta_{0\triangledown}^{vdW}\left[\frac{1}{(\kappa^{\triangledown})^4}\left(\frac{c_i^{\triangledown}}{c_{i0}^{\triangledown}}\right)^2 + \left(\frac{c_i^{\triangledown}}{4c_{i0}^{\triangledown}}\right)(\kappa^{\triangledown})^2 \mathrm{e}^{-2(\kappa^{\triangledown}-1)}\right. \\ &\quad \left. - \left(\frac{c_i^{\triangledown}}{c_{i0}^{\triangledown}}\right)^{3/2} \frac{\mathrm{e}^{-(\kappa^{\triangledown}-1)}}{\kappa^{\triangledown}}\right] = O\left(\Delta_{0\triangledown}^{vdw^2}\right), \\ &1 - \left(\frac{c_{i0}^{\triangledown}}{c_i^{\triangledown}}\right)^{1/2} \kappa^{\triangledown} \mathrm{e}^{-(\kappa^{\triangledown}-1)} + \Delta_{0\triangledown}^{vdW}\left[\frac{1}{5(\kappa^{\triangledown})^4}\left(\frac{c_i^{\triangledown}}{c_{i0}^{\triangledown}}\right)^2 + \left(\frac{c_i^{\triangledown}}{8c_{i0}^{\triangledown}}\right)(\kappa^{\triangledown}) \mathrm{e}^{-2(\kappa^{\triangledown}-1)}\right. \\ &\quad \left. - \left(\frac{c_i^{\triangledown}}{c_{i0}^{\triangledown}}\right)^{3/2} \frac{\mathrm{e}^{-(\kappa^{\triangledown}-1)}}{\kappa^{\triangledown}} m(\kappa)\right] = O\left(\Delta_{0\triangledown}^{vdw^2}\right), \end{aligned}\right\} \tag{B 3}$$

where $c_{i0}^{\triangledown}$ is given by (2.23), and

$$m(\kappa) = -\frac{\kappa^2}{2}\mathrm{e}^{\kappa}\,\mathrm{Ei}(-\kappa) + \frac{1-\kappa}{2}, \tag{B 4}$$

with Ei as the exponential integral function. In this formulation, $\Delta_{0\triangledown}^{vdW}$ is based on $\delta = \delta_0^{\triangledown}$. It can be shown that the expansions

$$\frac{c_i^{\triangledown}}{c_{i0}^{\triangledown}} = 1 - 0.053\Delta_{0\triangledown}^{vdW} + O\left(\Delta_{0\triangledown}^{vdw^2}\right), \tag{B 5}$$

$$\kappa^{\triangledown} = 1 + 0.223\Delta_{0\triangledown}^{vdW} + O\left(\Delta_{0\triangledown}^{vdw^2}\right) \tag{B 6}$$

are asymptotic solutions of (B 3) for $\Delta_{0\triangledown}^{vdw} \ll 1$. In particular, (B 5) represents the perturbation of the critical coagulation concentration (2.23) due to the substrate elasticity, and it shows that adhesion by electrolyte addition would occur at a lower concentration level in the hypothetical case in which elastic instabilities are negligible, which represents a good approximation in the range of validity of (B 5), $\Delta_0^{vdW} \ll \Delta_{0\triangledown}^{vdW} \ll 1$, and if $\Delta_{0\triangledown}^{vdW} < \Delta_{0C\triangledown}^{vdW}$. The value $\Delta_{0C\triangledown}^{vdW}$ represents the van der Waals compliance for elastostatic adhesion evaluated at the DLVO critical coagulation

conditions (2.22), and it can be obtained numerically by use of (B 1) and noticing that, in the first approximation, $\Delta_{0\triangledown}^{vdW} = \Delta_{0\triangledown}^{el}$ when $c_i^{\triangledown} = c_{i0}^{\triangledown}$ and $\kappa^{\triangledown} = \kappa_0^{\triangledown}$, from which $\Delta_{0C\triangledown}^{vdW} = 0.452$. However, if $\Delta_{0\triangledown}^{vdW} > \Delta_{0C\triangledown}^{vdW}$ elastostatic adhesion occurs before the particle has surpassed the small energy barrier, and the corrected DLVO criterion (B 5) loses accuracy. Equation (B 5) is consistent with the fact that substrate-deformation effects increase the effective value of the attractive forces and decrease that of the repulsive forces.

The onset of fluid flow by rotational or translational motion of the sphere produces a non-zero hydrodynamic pressure in the clearance, which alters the adhesion dynamics exposed in this appendix. These hydrodynamic effects are addressed in § 6.

REFERENCES

Berdan, C. & Leal, G. 1981 Motion of a sphere in the presence of a deformable interface. Part I. Perturbation of the interface from flat: the effects on drag and torque. *J. Colloid Interface Sci.* **87**, 62–80.

Berke, A. P., Turner, L., Berg, H. C. & Lauga, E. 2008 Hydrodynamic attraction of swimming microorgansims by surfaces. *Phys. Rev. Lett.* **101**, 038102.

Bike, S. G. & Prieve, D. C. 1995 The electrokinetic lift of a sphere moving in a slow shear flow parallel to a wall. *J. Colloid Interface Sci.* **175**, 422–434.

Busscher, H. J., Poortinga, A. T. & Bos, R. 1998 Lateral and perpendicular interaction forces involved in mobile and immobile adhesion of microorganisms on model solid surfaces. *Curr. Microbiol.* **37**, 319–323.

Cooley, M. D. A. & O'Neill, M. E. 1968 On the slow rotation of a sphere about a diameter parallel to a nearby plane wall. *J. Inst. Math. Appl.* **4**, 163–173.

Davis, R. H., Serayssol, J. M. & Hinch, E. J. 1986 The elastohydrodynamic collision of two spheres. *J. Fluid Mech.* **163**, 479–497.

Derjaguin, B. V. 1934 Analysis of friction and adhesion. Part IV. The theory of the adhesion of small particles. *Kolloid Zeits.* **69**, 155–164.

Derjaguin, B. V. & Landau, L. 1941 Theory of the stability of strongly charged lyophobic sols and the adhesion of strongly charged particles in solutions of electrolytes. *Acta Physicochim. URSS* **14**, 633–662.

Derjaguin, B. V., Muller, V. M. & Toporov, Y. P. 1975 Effect of contact deformations on adhesion of particles. *J. Colloid Interface Sci.* **53**, 314–326.

Goldman, A. J., Cox, R. G. & Brenner, H. 1967*a* Slow motion of a sphere parallel to a plane wall: Couette flow. *Chem. Engng Sci.* **22**, 653–660.

Goldman, A. J., Cox, R. G. & Brenner, H. 1967*b* Slow motion of a sphere parallel to a plane wall: motion through a quiescent fluid. *Chem. Engng Sci.* **22**, 637–651.

Hamaker, H. C. 1937 The London–van der Waals attraction between spherical particles. *Physica* **4** (10) 1058–1072.

Hu, H. H. & Joseph, D. D. 1999 Lift on a sphere near a plane wall in a second order fluid. *J. Non-Newton. Fluid Mech.* **88**, 173–184.

Israelachvili, J. N. 1985 *Intermolecular and Surface Forces*. Academic.

Johnson, K. L. 1985 *Contact Mechanics*. Cambridge University Press.

Johnson, K. L., Kendall, K. & Roberts, A. D. 1971 Surface energy and contact of elastic solids. *Proc. R. Soc. Lond.* A **324**, 301–313.

Landau, L. D. & Lifshitz, E. M. 1959 *Theory of Elasticity*. Pergamon Press.

Lauga, E., DiLuzio, W. R., Whitesides, G. M. & Stone, H. A. 2006 Swimming in circles: motion of bacteria near solid boundaries. *Biophys. J.* **90**, 400–412.

Leighton, D. & Acrivos, A. 1985 The lift on a small sphere touching a plane in the presence of a simple shear flow. *Z. Angew. Math. Phys.* **36**, 174–178.

Lifshitz, E. M. 1956 The theory of molecular attractive forces between solids. *Sov. Phys. JETP-USSR* **2**, 73–83.

Lyklema, J. 2005 *Fundamentals of Interface and Colloid Science, Vol. 4: Particulate Colloids*. Elsevier.

Meeker, S. P., Bonnecaze, R. T. & Cloitre, M. 2004 Slip and flow in pastes of soft particles: direct observation and rheology. *J. Rheol.* **48**, 1295–1320.

O'Neill, M. E. 1968 A sphere in contact with a plane wall in a slow linear shear flow. *Chem. Engng Sci.* **23**, 1293–1298.

O'Neill, M. E. & Stewartson, K. 1967 On the slow motion of a sphere parallel to a nearby plane wall. *J. Fluid Mech.* **27**, 705–724.

Poortinga, A. T., Bos, R., Norde, W. & Busscher, H. J. 2002 Electric double layer interactions in bacterial adhesion to surfaces. *Surf. Sci. Rep.* **47**, 1–32.

Saffman, P. G. 1964 The lift on a small sphere in a slow shear flow. *J. Fluid Mech.* **22**, 385–400.

Serayssol, J. M. & Davis, R. H. 1986 The influence of surface interactions on the elastohydrodynamic collision of two spheres. *J. Colloid Interface Sci.* **114**, 54–65.

Seth, J. R., Cloitre, M. & Bonnecaze, R. T. 2008 Influence of short-range forces on wall-slip in microgel pastes. *J. Rheol.* **52**, 1241–1268.

Skotheim, J. M. & Mahadevan, L. 2005 Soft lubrication: the elastohydrodynamics of nonconforming and conforming contacts. *Phys. Fluids* **17**, 1–23.

Trouilloud, R., Yu, T. S., Hosoi, A. E. & Lauga, E. 2008 Soft swimming: exploiting deformable interfaces for low Reynolds number locomotion. *Phys. Rev. Lett.* **101**, 048102.

Urzay, J., Llewellyn-Smith, S. G. & Glover, B. J. 2007 The elastohydrodynamic force on a sphere near a soft wall. *Phys. Fluids* **19**, 103106.

Verwey, E. J. W. & Overbeek, J. Th. G. 1948 *Theory of the Stability of Lyophobic Colloids*. Elsevier.

Vigeant, M. A. S., Ford, R. M. & Wagner, M. 2005 Reversible and irreversible adhesion of motile *Escherichia coli* cells analysed by total internal reflection aqueous fluorescence microscopy. *Appl. Environ. Microbiol.* **68**, 2794–2801.

Weekley, S. L., Waters, S. L. & Jensen, O. E. 2006 Transient elastohydrodynamic drag on a particle moving near a deformable wall. *Q. J. Mech. Appl. Math.* **59**, 277–300.

Wu, X., Warszynksi, P. & van de Ven, T. G. M. 1995 Electrokinetic lift: observations and comparisons with theories. *J. Colloid Interface Sci.* **180**, 61–69.